学位論文

Canonical approach to finite density QCD
(正準集合の方法を用いた有限密度格子 QCD 計算)

平成 28 年 12 月博士（理学）申請

東京大学大学院理学系研究科
物理学専攻　福田　龍太郎

Abstract

Although QCD has a rich phase structure at finite temperature and density, the investigations based on first–principles calculations are limited in small density regions due to so–called the sign problem. However, in finite–temperature and density QCD systems, a lot of physically interesting targets such as the early Universe, neutron stars and quark matters are waiting to be explored. Therefore, it is quite meaningful to seek for methods for accurate computation of thermodynamic quantities at large baryon chemical potential. This is an urgent subject also in the fields of particle and nuclear physics. The canonical approach which is studied in this thesis corresponds to a fugacity expansion of a grand canonical partition function and it could have a potential to overcome the sign problem. However, it is reported that it has its particular numerical difficulties and it is somewhat unclear whether it can produce reliable results. Taking this situation into consideration, in this thesis, the author discusses the validity of the canonical approach and calculates the pressure, the baryon number density, and the baryon susceptibility at finite density through lattice QCD simulation based on the canonical approach. The results are also compared with those obtained using the multi–parameter reweighting method and the Taylor expansion method on the lattice which are considered as the valid method for finite density QCD at a small baryon chemical potential. The results obtained by the canonical approach are found to be in very good agreement in the regions where the statistical errors in the multi–parameter reweighting method and Taylor expansion method are under control. Moreover, our canonical approach works beyond $\mu_B/T \simeq 3$ while the validity range of other lattice method for finite density QCD is practically limited to $\mu_B/T \lesssim 3$.

Contents

Chapter 1

Introduction

In this chapter, basic concepts of quantum chromodynamics (QCD) are first overviewed and then a theoretical conjecture of the QCD phase diagram on a temperature–baryon chemical potential plane is introduced. Because we have no definitive method based on first–principles calculation at present to analyze the QCD phase diagram, proposed QCD phase diagrams so far have a lot of uncertainties.

1.1 QCD in a nutshell

Quantum chromodynamics (QCD) is the theory of strong interaction. The QCD Lagrangian in Euclidian space is given with bare coupling constant g and quark mass m_f as follows;

$$L_{\rm QCD} = \frac{1}{4}F^a_{\mu\nu}F^a_{\mu\nu} + \sum_{f,a}\bar{\psi}^a_f(D_\mu\gamma_\mu + m_f)\psi^a_f. \tag{1.1}$$

The indices a and f on the quark field are the degrees of freedom of color and flavor, respectively. Here, $F^a_{\mu\nu}$ is a tensor called the field strength defined with a gluon field A^a_μ as follows;

$$F^a_{\mu\nu} = \partial_\mu A_\nu + igf^{abc}A^b_\mu A^c_\nu. \tag{1.2}$$

The degree of freedom of color on the gluon field is $N_c^2 - 1$ and the degree of freedom of color on a quark field N_c. Here, f^{abc} is the structure constant defined with generators λ^a of Lie group $SU(N_c)$ as follows;

$$[\lambda^b, \lambda^c] = if^{abc}\lambda^a. \tag{1.3}$$

$D_\mu\gamma_\mu$ is called Dirac operator and the definition is

$$D_\mu\gamma_\mu = (\partial_\mu + igA^a_\mu\lambda^a)\gamma_\mu. \tag{1.4}$$

The second term in the Dirac operator corresponds to the term describing the interaction between quarks and gluons. It is considered that there are six quark flavors (up, down, charm, strange, top, and bottom). In theoretical calculations of QCD in thermal equilibrium, only two flavors (i.e. up and down) or three flavors (i.e. up, down, and strange) are usually included. This is because these quark masses are lighter than $\Lambda_{\rm QCD} \sim 200$MeV which is the typical energy scale of QCD. According to the Particle Data Group [1] these quark masses reads,

$$m_u = 2.2^{+0.6}_{-0.4} \ \ \text{MeV}, \tag{1.5}$$

$$m_d = 4.7^{+0.5}_{-0.4} \ \ \text{MeV}, \tag{1.6}$$

$$m_s = 96^{+8}_{-4} \ \ \text{MeV}. \tag{1.7}$$

Moreover, only up and down quarks with approximately degenerated mass are often considered in lattice QCD formalism. This type of lattice QCD formalism is called 2–flavor lattice QCD.

The QCD Lagrangian is invariant under the following local gauge transformation;

$$\psi(x) \to \Omega(x)\psi(x), \tag{1.8}$$

$$A_\mu \to \Omega(x)A_\mu(x)\Omega^{-1}(x) - \frac{i}{g}\Omega(x)\partial_\mu\Omega^{-1}(x). \tag{1.9}$$

Here, $\Omega(x) \in SU(3)$ and $A_\mu(x) = A^a_\mu(x)\lambda^a \in su(3)$.

1.2 Conjecture of QCD phase diagram at finite temperature and density

QCD has the property called asymptotic freedom [2, 3]. This is the phenomenon that the magnitude of the coupling constant g depends on the energy scale of a QCD system due to the polarizations of gluons. Using the one–loop calculation, the effective coupling constant $\alpha_s(Q)$ is given as follows;

$$\alpha_s(Q) = \frac{12\pi}{(33 - 2N_f)\log\left(\frac{Q^2}{\Lambda_{\rm QCD}}\right)}. \tag{1.10}$$

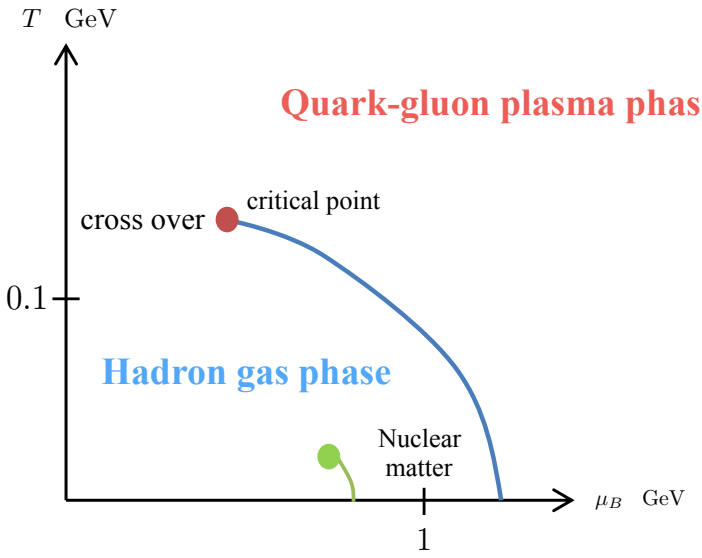

Figure 1.1: Conjecture of QCD phase diagram at finite temperature and density. The Blue line indicates the phase transition line between confining and deconfining phase and the red point corresponds to the critical point of the transition. The green line is the liquid–gas phase transition.

Here, Q is the energy scale we are interested in. From this expression, we can say that the effective coupling constant decreases as Q increases. This fact suggests that the quark–gluon plasma phase where quarks almost freely move realizes at high temperature and the hadronic phase where quarks form bound states realizes at low temperature. Figure 1.1 is one of conjectures of the QCD phase diagram at finite temperature and density. Some phenomenological models predict that low density and high temperature region corresponds to the quark–gluon plasma phase and low temperature region corresponds to the hadronic phase [4]. The phase transition between confining and deconfining phase at vanishing baryon density has been discussed in detail by lattice QCD calculation. For the realistic QCD case with up, down, and strange quark with physical quark masses, it is established that the phase transition is crossover from analysis using staggered fermions and Wilson fermions [6, 7]. Considering lattice spacing dependence and volume dependence of thermodynamic observables, we have strong evidences to conclude that the typical value of pseudo critical temperature is $150 - 200$ MeV.

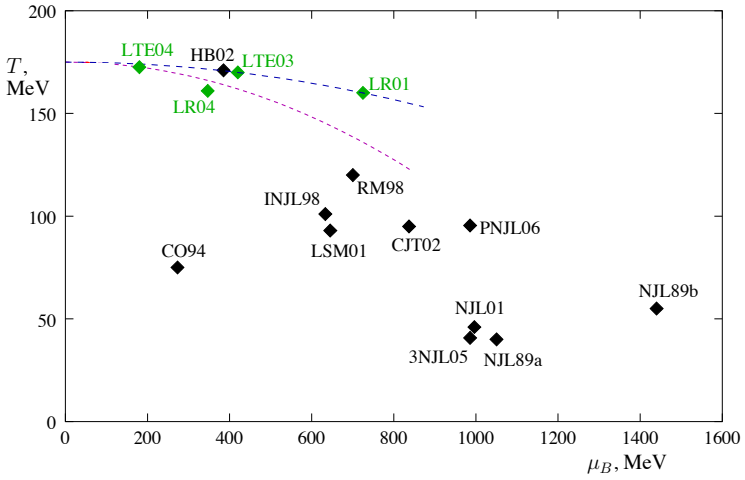

Figure 1.2: Theoretical predictions for the location of the critical point of the QCD phase diagram. This figure is adopted from the reference [13]. The label of the points are explained in the table 1.1. The blue and magenta dashed lines correspond to the slopes of $d^2T/d\mu_B^2$ of the transition line evaluated by lattice simulation at vanishing baryon chemical potential.

The most recent lattice QCD simulation using $2+1$ flavors with physical quark masses indecates that T_c is 155(1)(8) MeV [8]. A lot of chiral models indicate that the "QCD critical point" of chiral phase transition line at (T_{cp}, μ_{cp}) in Fig.1.1 exits on the QCD phase diagram. This means that the phase transition is crossover for $\mu_B < \mu_{pc}$ and first order for $\mu_B > \mu_{pc}$ for physical up, down, and strange quark masses [9, 10, 11, 12]. Thus, the phase transition at the QCD critical point is second order. The predicted QCD critical points are widely spread on the QCD phase diagram as shown in Fig.1.2 and there are some models which predict that the critical point does not exist in finite temperature and density QCD.

Near the phase transition line between confining and deconfining phase transition, we expect that anomalous features of observables closely related to the phase transition occur. For example, an order parameter to characterize the QCD critical point is the chiral condensate $\langle \bar{\psi}\psi \rangle$ and the correlation length and the fluctuation diverge at the critical point. The fluctuation of the baryon number at finite baryon chemical potential μ_B with finite quark mass also diverges at the critical point because the baryon number couples with

Table 1.1: Labels for Fig.1.2. This table is adopted from [13].

Label	Technique	Source
NJL89a	Nanbu–Jona–Lasinio (NJL)	[9]
NJL89b	NJL	[9]
CO94	Composite operator	[10, 14, 15]
INJL98	Instanton NJL	[12]
RM98	Random matrix	[16]
LSM01	Linear sigma model	[17]
NJL01	NJL	[17]
HB02	Hadronic boostrap	[18]
CJT02	Effective potential	[19]
3NJL05	3–flavor NJL	[20]
PNJL06	NJL with Polyakov loop	[21]
LR01	Lattice multi–parameter reweighting	[22]
LR04	Lattice multi–parameter reweighting	[23]
LTE03	Lattice Taylor expansion	[24]
LTE04	Lattice Taylor expansion	[25]

the chiral condensate. This fluctuation can be explained physically as the response of the baryon number density to an infinitesimal change of baryon chemical potential. Therefore, the behavior of the baryon susceptibility χ_B which is the first order derivative of the baryon number density in terms of baryon chemical potential is important and a chiral effective model actually tells us that the baryon number susceptibility shows a peak on the crossover line between the chiral broken and symmetric phases on a QCD phase diagram. Figure 1.3 is an example of this feature. Here, let us focus on the relation between high energy experiments with accelerators and theoretical trials for searching for the chiral phase transition and the critical point. Interesting quantities for this purpose include higher order cumulants of conserved charges. They are sensitive to the correlation length [29] and they behave anomalously around the critical point. The higher baryon number cumulants χ_{n+1} are given as follows.

$$\chi_{n+1} = \frac{\langle N^{n+1} \rangle_c}{V} = \frac{\partial}{\partial(\mu_B/T)} \frac{\langle N^{n+1} \rangle_c}{V} = \frac{\chi_n}{\partial(\mu_B/T)} \tag{1.11}$$

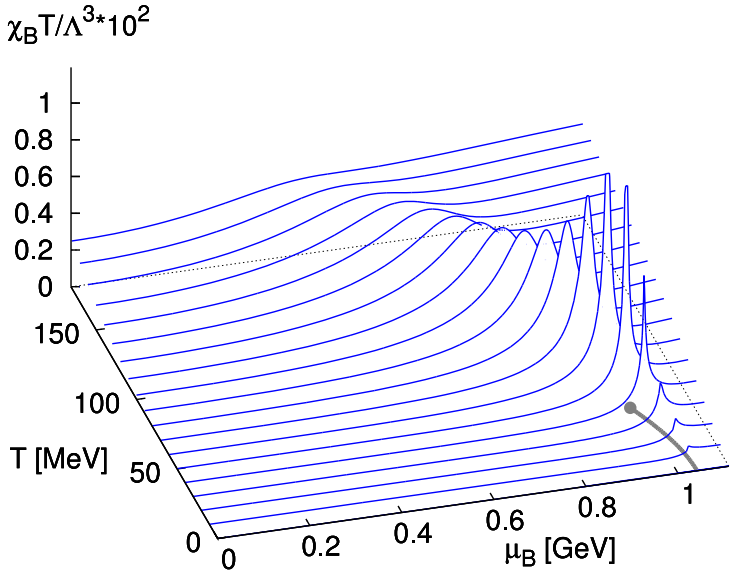

Figure 1.3: Temperature T and baryon chemical potential μ_B dependence of baryon number susceptibility χ obtained by the 2–flavor Nambu–Jona–Lasinio model [26, 27]. This figure is taken from [28]. The bold line in this figure corresponds to the first order phase transition and the end of this line indicates the critical point.

In particular, χ_2 is just the baryon number susceptibility χ_B.

$$\chi_2 = \frac{\langle N^2 \rangle_c}{V} = \frac{\partial}{\partial(\mu_B/T)} \frac{\langle N \rangle}{V} \tag{1.12}$$

From this definition, we can conclude that the signs of χ_3 and χ_4 change around the phase transition line due to the behavior of χ_2 [28]. In high energy experiments, skewness S and kurtosis K defined below have been measured by event–by–event analysis to pick up the anomalous behavior of the fluctuation of observables. The definition of the skewness is,

$$S = \frac{\langle N^3 \rangle_c}{\chi_2^3}, \tag{1.13}$$

and the definition of the kurtosis is,

$$K = \frac{\langle N^4 \rangle_c}{\chi_2^4}. \tag{1.14}$$

The skewness and the kurtosis also give us important information; these quantities show sign flip near the QCD critical point. In event–by–event analysis in relativistic heavy ion collisions, the numbers of specific particles are measured in each event. For example, the net–proton distribution has been observed by STAR Collaboration as shown in Fig.1.4. From this result, we can extract the probability distribution function for the particle and we can evaluate the skewness and the kurtosis [31, 32]. Ideally, this measurement of the net–proton distribution should be replaced by the measurement of the net–baryon distribution because the net–proton number is not a conserved charge. However, measuring the net–baryon number is quite difficult because detectors cannot identify neutral baryons.

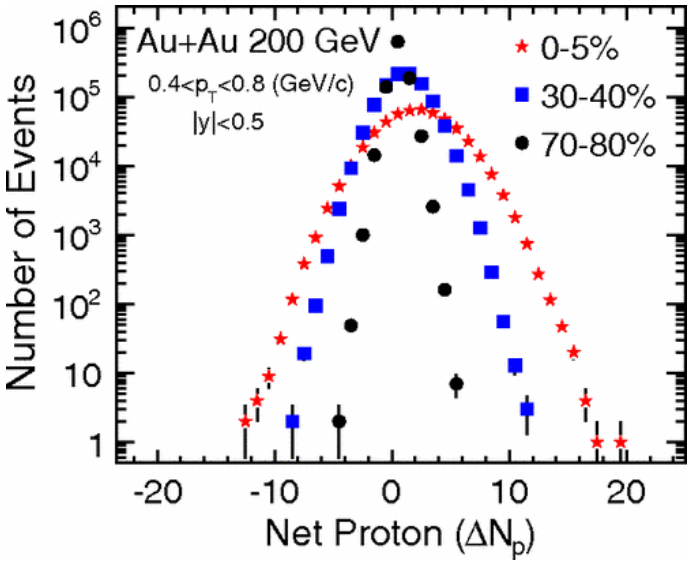

Figure 1.4: Net–proton number distribution measured by STAR Collaboration. This figure is taken from [30].

1.3 Purpose of the present thesis

As stated in previous chapter, there are lots of physically interesting targets of QCD on a temperature–baryon density plane. For example, in addition to the topics (chiral phase transition and QCD critical point) explained in the

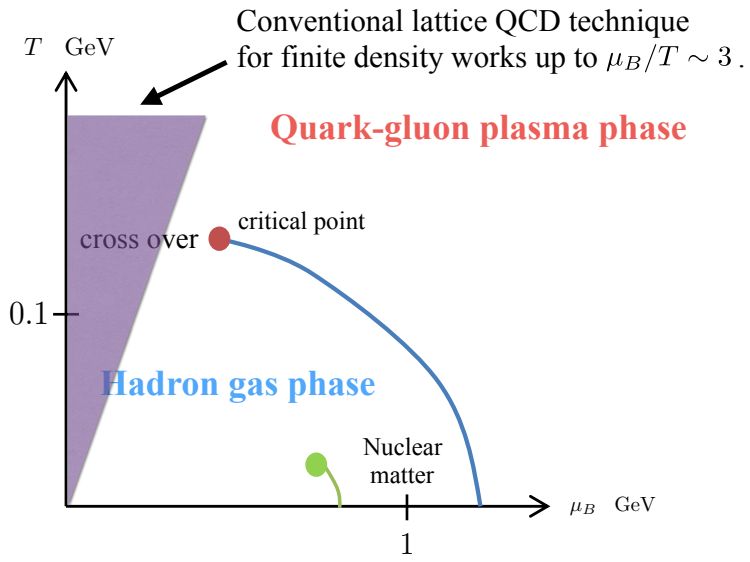

Figure 1.5: Region where conventional lattice QCD technique for finite density works on a temperature–baryon density plane.

previous chapter, the early Universe, neutron stars, and quark matter could be relevant to the QCD phase diagram research [4].

At this stage, we have the multi–parameter reweighting method [22, 33] and the Taylor expansion method [34, 35, 36], the imaginary chemical potential method [37, 38], and the density of states method [39, 40, 41] as major approaches to finite density QCD from first–principles calculation. However, it is considered that these methods are valid only for QCD with a small chemical potential which corresponds to QCD in low density region. To be more specific, it is empirically known that these methods safely work only up to $\mu_B/T \sim 3$, where μ_B is a baryon chemical potential. This restriction comes from the so–called sign problem [4, 42, 43] discussed in Chapter 4 in detail. Therefore, it is highly important to explore other methods for investigating finite-density QCD systems quantitatively from *ab initio* calculations; this is also an urgent subject in the fields of particle and nuclear physics.

In this thesis, the canonical approach to finite density lattice QCD [44, 45, 46, 47, 48, 49] is adopted and studied. The main reasons are as follows.

1. The canonical approach can avoid the sign problem in principle.

In the canonical approach, first we compute a set of canonical partition functions and then we construct a fugacity expansion of a grand canonical partition function. Canonical partition functions can be calculated through the Fourier transformation of the grand canonical partition functions calculated at purely imaginary chemical potential. This procedure does not suffer from the sign problem.

2. The canonical approach can relate theoretical results and experimental results directly.

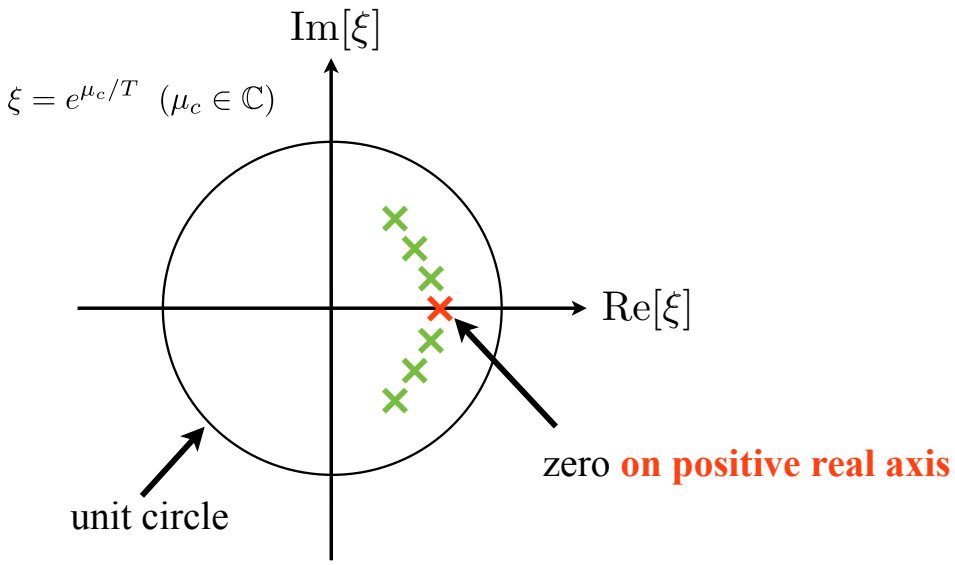

Figure 1.6: Conceptual diagram of Lee–Yang zeros. Cross marks indicate the zero points of a grand canonical partition function with a complex chemical potential.

For instance, the canonical partition functions Z_n are closely related to a multiplicity distribution of protons $P(n = N_p - N_{\bar{p}})$ where N_p and $N_{\bar{p}}$ are the numbers of protons and anti-protons, respectively, measured at Brookhaven National Laboratory [50] as follows;

$$Z_n e^{n\mu/T} = P(n, \mu/T). \tag{1.15}$$

That is, using the canonical approach allows for a unique suggestion for experiments that cannot be obtained from other methods. Thus,

we can extract information on the phase transition from results of the experiment with the canonical approach using Lee–Yang zeros analysis [51]. The Lee–Yang zeros analysis can be performed as follows. Considering the fugacity expansion of the grand canonical partition function $Z_{GC}(\mu_c)$ with complex chemical potential μ_c, we can search the zero points h_i of the grand canonical partition function,

$$Z_{GC}(T, \mu_c) = \prod_i (e^{\mu_c/T} - h_i). \tag{1.16}$$

These zero points h_i are called the Lee–Yang zeros and the distribution on a fugacity plane includes information of the phase structure of the corresponding statistical system. In thermodynamic limit, the number of zeros becomes infinite and the zeros coalesce onto one–dimensional curves on a fugacity plane as shown in Fig.1.6. If a system has first order phase transition at μ/T, the coalescing zero points touch the phase transition point on a positive real axis on a fugacity plane. On the other hand, if a system has second order phase transition, the coalescing zero points pinch the point. In case of crossover, coalescing zeros do not reach to the point. Therefore, we can indentify a phase transition point and the order using this analysis. In actual numerical simulation, it is important to analyze the volume dependence of Lee-Yang zeros because no zero point appears on the real axis for a finite volume system.

Considering above, it can be said that the canonical approach could be a hopeful candidate to analyze the thermodynamics of QCD at large baryon density. The main purpose of this thesis is to check if the canonical approach could work for finite-density QCD in an actual numerical simulation. The canonical approach has not only the good points as stated above but some problems also. To search for clues to overcome these problems, we will make comprehensive and quantitative estimates using the canonical method.

In this thesis, chapter 2 is devoted to the formulation of quantum field theory on a lattice at zero temperature and vanishing density. In chapter 3, brief descriptions of finite temperature and density QCD on a lattice are given and the sign problem is also explained in detail. In chapter 4, conventional lattice QCD methods including the canonical approach for finite density QCD are briefly explained. Chapters 2–4 correspond to the review part of my thesis. In Chapter 5, difficulties of the canonical approach are discussed and

my new solutions for them are also presented. This part is mainly based on the following paper.

- Ryutaro Fukuda, Atsushi Nakamura, and Shotaro Oka, "Canonical approach to finite density QCD with multiple precision computation" Phys. Rev. D **93**, 094508 (2016) [52]

In chapter 6, my numerical set up is first given and then the validity of my new solutions for the difficulties of the canonical approach is discussed. After that, results of the thermodynamic observables such as the pressure, the baryon number density, and the baryon susceptibility from my strategy are presented and compared to preceding works in chapter 5. This part is mainly based on [52] and the following paper.

- Ryutaro Fukuda, Atsushi Nakamura, and Shotaro Oka, "Validity range of canonical approach to finite density QCD" Proceeding of Science (LATTICE 2015) 167 (2015) [53]

Thus, chapters 5 and 6 correspond to the description of my original work.

Chapter 2

Lattice field theory at zero temperature and vanishing density

In this chapter, a method for introducing interaction fermions at zero temperature and vanishing density on a lattice is shortly explained. The clue which can support us to achieve it is an invariance under the local gauge transformation that QCD on a lattice should hold.

2.1 Naive QCD action on a lattice

2.1.1 Fermionic part of the QCD action on a lattice

As stated in the previous chapter, the fermionic part $S_F[\psi, \bar{\psi}, A]$ of the QCD action in Euclidian space is given by a bilinear functional in the quark fields ψ and $\bar{\psi}$ as follows;

$$S_F[\psi, \bar{\psi}, A] = \sum_{f=1}^{N_f} \int dx^4 \bar{\psi}^f(x)^a_\alpha \Big[(\gamma_\mu)_{\alpha\beta} (\delta^{ab}\partial_\mu + iA_\mu(x)^{ab}) + m^f \delta_{\alpha\beta}\delta^{ab} \Big] \psi(x)^b_\beta. \tag{2.1}$$

Before considering the discretization of interacting fermions, we discuss the discretization of free fermions. After this step, we introduce gauge fields on a lattice.

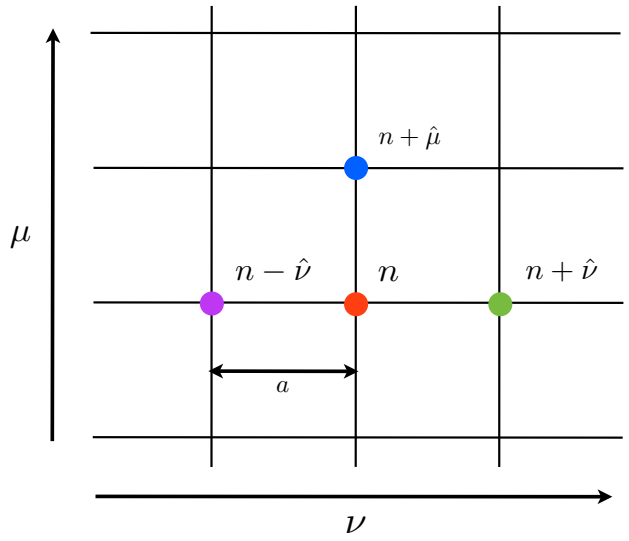

Figure 2.1: Discretization of spacetime coordinates. n indicates a spacetime coordinate (n_1a, n_2a, n_3a, n_4a) on a lattice with a lattice spacing of a. μ and ν simply present the orientation of the spacetime coordinate. Note that $n \pm \hat{\mu}$ corresponds to $(n_1a, n_2a, n_3a, n_4a) \pm (\delta_{\mu 1}a, \delta_{\mu 2}a, \delta_{\mu 3}a, \delta_{\mu 4}a)$.

Free fermions

In the continuum theory, the free single flavor fermion action S_F^{free} is given by the expression

$$S_F^{\text{free}}[\psi, \bar{\psi}] = \int dx^4 \bar{\psi}(x)\Big(\gamma_\mu \partial_\mu + m\Big)\psi(x). \tag{2.2}$$

On a lattice, we need to discretize space–time coordinates (see Fig.2.1) so that discretized ones can be labeled sets of four integer numbers $n = (n_1, n_2, n_3, n_4)$ which run from 1 to N_μ. Therefore, the corresponding lattice volume V can be calculated as $(N_x a) \times (N_y a) \times (N_z a) \times (N_t a)$ with a lattice spacing a. Using the following symmetric discretized derivative

$$\partial_\mu \psi(n) \sim \frac{\psi(n+\hat{\mu}) + \psi(n-\hat{\mu})}{2a} \tag{2.3}$$

and discretized 4–dimensional integration

$$\int dx^4 \sim a^4 \sum_{n_x=1}^{N_x} \sum_{n_y=1}^{N_y} \sum_{n_z=1}^{N_z} \sum_{n_t=1}^{N_t} \equiv a^4 \sum_n , \tag{2.4}$$

the free fermion action on a lattice can be given by

$$S_F^{\rm free}[\psi,\bar{\psi}] = a^4 \sum_n \bar{\psi}(n) \left(\sum_{\mu=1}^{4} \gamma_\mu \frac{\psi(n+\hat{\mu}) - \psi(n-\hat{\mu})}{2a} + m\psi(n) \right). \quad (2.5)$$

This is the starting point for a discretized fermionic part for the interacting case of Eq.(2.1) on a lattice.

Interacting case

To consider an interacting fermion case, as in the continuum theory, we need to take into account the invariance of the action under the following local gauge transformation with a $SU(3)$ matrix $\Omega(x)$;

$$\psi(x) \to \psi'(x) = \Omega(x)\psi(x), \quad (2.6)$$

$$\psi(\bar{x}) \to \bar{\psi}'(x) = \bar{\psi}(x)\Omega^\dagger(x). \quad (2.7)$$

We can easily find that the mass term in Eq.(2.5) is invariant under this transformation. On the other hand, the discretized derivative term is not gauge invariant. Therefore, we need to introduce a field $U_\mu(x)$ to keep the term invariant under the transformation. To be more specific, we consider

$$\bar{\psi}(n)U_{\pm\mu}(n)\psi(n \pm \hat{\mu}) \quad (2.8)$$

instead of $\bar{\psi}(n)\psi(n \pm \hat{\mu})$ in Eq.(2.5). This new term with $U_{\pm\mu}$ is transformed under the gauge transformation as follows;

$$\bar{\psi}'(n)U'_{\pm\mu}(n)\psi'(n \pm \hat{\mu}) = \bar{\psi}(n)\Omega^\dagger(n)U'_{\pm\mu}(n)\Omega(n \pm \hat{\mu})\psi(n \pm \hat{\mu}). \quad (2.9)$$

Consequently, $\bar{\psi}(n)U_{\pm\mu}(n)\psi(n\pm\hat{\mu})$ becomes gauge invariant if we regard that the gauge transformation of $U_{\pm\mu}(n)$ is given by

$$U'_{\pm\mu}(n) = \Omega(n)U_{\pm\mu}(n)\Omega^\dagger(n \pm \hat{\mu}). \quad (2.10)$$

Therefore, the interacting fermionic action can be given by the following form;

$$S_F = a^4 \sum_n \bar{\psi}(n) \left(\sum_{\mu=1}^{4} \gamma_\mu \frac{U_\mu(n)\psi(n+\hat{\mu}) - U_{-\mu}(n)\psi(n-\hat{\mu})}{2a} + m\psi(n) \right). \quad (2.11)$$

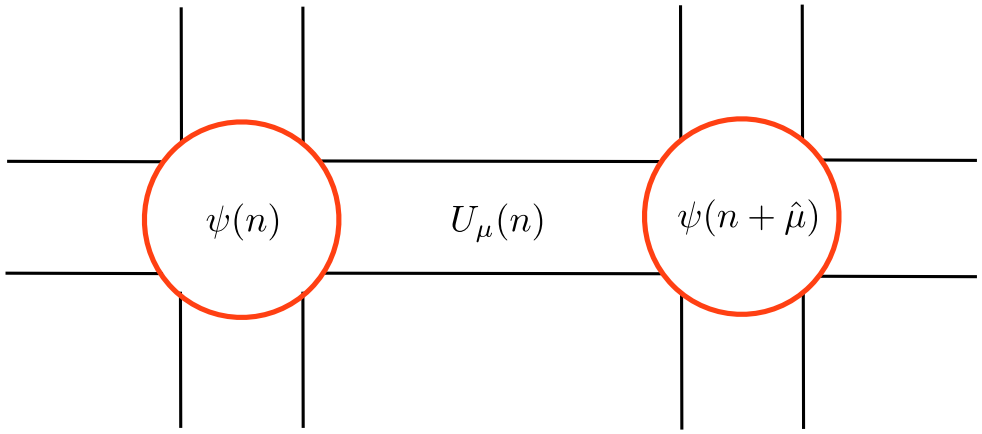

Figure 2.2: Location of fermion fields ψ and link variables U_μ on a lattice. Fermion fields live on a discretized point and link variables are attached geometrically on a link of a lattice.

This fermionic action holds the gauge invariant property thanks to the matrix U_μ. This matrix $U_\mu(n)$ is called a link variable because this has an orientation μ and can be considered to be attached geometrically on a link of a lattice as shown in Fig.2.2. We also easily find that $U_{-\mu}(n)$ is equivalent to $U_\mu^\dagger(n-\hat{\mu})$. In the following section, the relation between a link variable U_μ and a gauge field A_μ is discussed.

2.1.2 Gauge part of the QCD action on a lattice

Constructing the gauge part of the QCD action on a lattice, it is crucial to make use of the plaquette $U_{\mu\nu}(n)$ which is a closed loop composed by a product of four link variables. This plaquette is defined as

$$U_{\mu\nu}(n) = U_\mu(n)U_\nu(n+\hat{\mu})U_\mu^\dagger(n+\hat{\nu})U_\nu^\dagger(n) \tag{2.12}$$

and this can be sketched as shown in Fig.2.3. Using this plaquette, the gauge part of the QCD action on a lattice can be given by

$$S_G^W[U] = \frac{2}{g^2}\sum_n\sum_{\mu<\nu}\mathrm{Re}\,\mathrm{tr}[1-U_{\mu\nu}(n)] \tag{2.13}$$

and this type of the gauge action was introduced by Wilson for the first time [54]. Thus, this gauge action is usually called Wilson gauge action. The

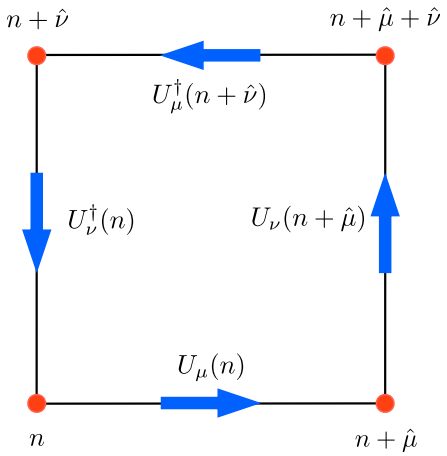

Figure 2.3: Schematical view of a plaquette. A plaquette at n is the closed loop from n composed by a product of four link variables.

problem we have to consider is if this gauge action is gauge invariant and it can produce the continuum gauge action when taking a continuum limit $a \to 0$.

Gauge invariance of Wilson gauge action

We have only to check if the trace of a plaquette is gauge invariant for making sure that Wilson gauge action is gauge invariant;

$$\mathrm{tr}\, U'_{\mu\nu}(n) = \mathrm{tr}\, [\Omega(n) U_\mu(n) U_\nu(n+\hat{\mu}) U_\mu^\dagger(n+\hat{\nu}) U_\nu^\dagger(n) \Omega^\dagger(n)] = \mathrm{tr}\, U_{\mu\nu}(n). \tag{2.14}$$

Therefore, it can be said that Wilson gauge action is gauge invariant.

Continuum limit of Wilson gauge action

First of all, we need to discuss the relation between a link variable U_μ and a gauge field A_μ to study the continuum limit of Wilson gauge action of (2.13). The starting point is the gauge transformation of a link variable of (2.10). In the continuum theory, it is known that the following quantity

$T(x,y)$ is transformed in the same way as a link variable under the gauge transformation;

$$\begin{aligned} T(x,y) &= \mathrm{P}\exp\left(i\int_x^y A_\mu(z)dz^\mu\right) \\ &= \lim_{N\to\infty}\prod_{n=0}^{N-1}\Big(1+iA_\mu(x_n)\Delta x^\mu\Big), \end{aligned} \tag{2.15}$$

where x_n and $|\Delta x|$ are defined by $x+n\Delta x$ and $|y-x|/N$, respectively. Let us actually check the gauge transformation of $T(x,y)$;

$$T'(x,y) = \lim_{N\to\infty}\prod_{n=0}^{N-1}\Big(1+iA'_\mu(x_n)\Delta x^\mu\Big), \tag{2.16}$$

$$A'_\mu(x_n) = \frac{1}{i}\Omega(x_n)\partial_\mu\Omega^\dagger(x_n) + \Omega(x_n)A_\mu(x_n)\Omega^\dagger(x_n). \tag{2.17}$$

Therefore, we can reach to the expression

$$\begin{aligned} 1+iA'_\mu(x_n)\Delta x^\mu &= 1+\Omega(x_n)\partial_\mu\Omega^\dagger(x_n)\Delta x^\mu + i\Omega(x_n)A_\mu(x_n)\Omega^\dagger(x_n)\Delta x^\mu \\ &= \Omega(x_n)\Big(1+iA_\mu(x_n)\Delta x^\mu\Big)\Omega^\dagger(x_{n+1}) + O\Big((\Delta x)^2\Big). \end{aligned} \tag{2.18}$$

To obtain the second line of Eq.(2.18), the expressions

$$\partial_\mu\Omega^\dagger(x_n)\Delta x^\mu = \Omega^\dagger(x_{n+1}) - \Omega^\dagger(x_n), \tag{2.19}$$

$$\Omega^\dagger(x_{n+1}) = \Omega^\dagger(x_n) + O(\Delta x) \tag{2.20}$$

are used. Consequently, we can get the following gauge transformation;

$$T'(x,y) = \Omega(x)T(x,y)\Omega^\dagger(y). \tag{2.21}$$

Taking into account this similarity between U_μ and T, we can conclude that $U_\mu(n)$ is equivalent to $T(n,n+\hat{\mu})$ in case of an enough small lattice spacing. This apparently means that a link variable can be written with a gauge field A_μ as follows;

$$U_\mu(n) = \exp\Big(iaA_\mu(n)\Big). \tag{2.22}$$

Using the relation (2.22) between a link variable and a gauge field, let us consider the continuum limit of Wilson gauge action. Plaquettes in Wilson gauge action can be expanded with Baker–Campbell–Hausdorff formula

$$\exp(X)\exp(Y) = \exp\Big(X + Y + \frac{1}{2}[X,Y] + \cdots\Big), \tag{2.23}$$

where X and Y are arbitrary matrices. Then, we obtain

$$\begin{aligned}
U_{\mu\nu}(n) &= e^{iaA_\mu(n)} e^{iaA_\mu(n+\hat{\mu})} e^{-iaA_\mu(n+\hat{\nu})} e^{-iaA_\nu(n)} \\
&= \exp\Big[iaA_\mu(n) + iaA_\nu(n+\hat{\mu}) - iaA_\mu(n+\hat{\nu}) - iaA_\nu(n) \\
&- \frac{a^2}{2}[A_\mu(n), A_\nu(n+\hat{\mu})] + \frac{a^2}{2}[A_\mu(n), A_\mu(n+\hat{\nu})] \\
&+ \frac{a^2}{2}[A_\nu(n+\hat{\mu}), A_\mu(n+\hat{\nu})] + \frac{a^2}{2}[A_\mu(n), A_\nu(n)] \\
&+ \frac{a^2}{2}[A_\nu(n+\hat{\mu}), A_\nu(n)] - \frac{a^2}{2}[A_\mu(n+\hat{\nu}), A_\nu(n)] + O(a^3)\Big] \\
&= \exp\Big[ia^2\Big(\partial_\mu A_\nu(n) - \partial_\nu A_\mu(n) + i[A_\mu(n), A_\nu(n)]\Big) + O(a^3)\Big] \\
&= \exp\Big[ia^2 F_{\mu\nu} + O(a^3)\Big].
\end{aligned} \tag{2.24}$$

The expansion

$$A_\mu(n+\hat{\nu}) = A_\mu(n) + a\partial_\nu A_\mu(n) + O(a^2) \tag{2.25}$$

is repeatedly used to get the third line from the second line in Eq.(2.24). Using the expression (2.24), Wilson gauge action can be written in terms of a field strength $F_{\mu\nu}$;

$$\begin{aligned}
S_G^W[A] &= \frac{2}{g^2}\sum_n \sum_{\mu<\nu} \mathrm{Re\ tr}\Big[1 - \exp\big(ia^2 F_{\mu\nu}\big)\Big] \\
&= \frac{1}{g^2}\sum_n \sum_{\mu=1}^{4}\sum_{\nu=1}^{4} \mathrm{Re\ tr}[-ia^2 F_{\mu\nu}(n) + a^4 F_{\mu\nu}^2] + O(a^2) \\
&= \frac{a^4}{2g^2}\sum_n \sum_{\mu=1}^{4}\sum_{\nu=1}^{4} \mathrm{tr}\ F_{\mu\nu}^2.
\end{aligned} \tag{2.26}$$

Getting the third line in Eq.(2.26), two relations $\mathrm{Re}X = (X + X^\dagger)/2$ and $U_{\mu\nu}^\dagger = U_{\nu\mu}$ are used. Thus, we can conclude that Wilson gauge action is equivalent to the continuum gauge action in the continuum limit.

2.1.3 Summary: naive QCD action on a lattice

From the above discussion, the naively discretized QCD action on a lattice can be given by

$$S_{QCD}^{naive} = a^4 \sum_n \bar{\psi}(n) \left(\sum_{\mu=1}^{4} \gamma_\mu \frac{U_\mu(n)\psi(n+\hat{\mu}) - U_{-\mu}(n)\psi(n-\hat{\mu})}{2a} + m\psi(n) \right) + \frac{2}{g^2} \sum_n \sum_{\mu<\nu} \mathrm{Re\ tr}[1 - U_{\mu\nu}(n)]. \tag{2.27}$$

Unfortunately, this is not appropriate as an interacting single flavor fermion action on a lattice because the fermion part of the naive QCD action has the problem called the fermion doubling. In the next section, the doubling problem is explained and one solution is also introduced.

2.2 Fermion doubling and Wilson fermion action

2.2.1 Fermion doubling

For studying the fermion part of the naive QCD action in more detail, we rewrite the fermion part in the following style;

$$S_F[\psi, \bar{\psi}, U] = a^4 \sum_{n,m} \sum_{c,d} \sum_{\alpha,\beta} \bar{\psi}(n)^c_\alpha D(n|m)^{cd}_{\alpha\beta} \psi(m)^d_\beta, \tag{2.28}$$

$$D(n|m)^{cd}_{\alpha\beta} = \sum_{\mu=1}^{4} (\gamma_\mu)_{\alpha\beta} \frac{U_\mu(n)^{cd}\delta_{n+\hat{\mu},m} - U_{-\mu}(n)^{cd}\delta_{n-\hat{\mu},m}}{2a} + m\delta_{\alpha\beta}\delta^{cd}\delta_{nm}. \tag{2.29}$$

Let us see the Dirac operator for free case ($U_\mu(n) = 1$ for all n) in momentum space using the Fourier transformation;

$$\begin{aligned} \tilde{D}(p|q) &= \frac{1}{N_x N_y N_z N_t} \sum_{n,m} e^{-ip\cdot na} D(n|m) e^{iq\cdot ma} \\ &= \delta(p-q)\Big(m + \frac{i}{a} \sum_{\mu=1}^{4} \gamma_\mu \sin(p_\mu a) \Big) \\ &= \delta(p-q)\tilde{D}(p). \end{aligned} \tag{2.30}$$

This expression means that the Dirac operator is diagonal in momentum space for free case. Moreover, the inverse of the Dirac operator in momentum space can be computed easily as follows;

$$\begin{aligned}\tilde{D}^{-1}(p) &= \frac{1}{m + \frac{i}{a}\sum_{\mu=1}^{4}\gamma_\mu \sin(p_\mu a)} \\ &= \frac{m - \frac{i}{a}\sum_{\mu=1}^{4}\gamma_\mu \sin(p_\mu a)}{m^2 + \frac{1}{a^2}\sum_{\mu=1}^{4}\sin^2(p_\mu a)}.\end{aligned} \tag{2.31}$$

To simplify our discussion, let us consider massless fermions. For this case in the continuum limit, Eq.(2.31) becomes

$$\tilde{D}^{-1}(p; m = 0, a \to 0) = \frac{-i\sum_{\mu=1}^{4}\gamma_\mu p_\mu}{p^2}. \tag{2.32}$$

This propagator has a pole at $p = (0, 0, 0, 0)$ and this corresponds to a single flavor massless fermion. Therefore, this propagator is surely correct in the continuum limit as expected. However, the propagator in momentum space on a lattice has a fatal problem. The expression

$$D^{-1}(p; m = 0, a \neq 0) = \frac{-ia\sum_{\mu=1}^{4}\gamma_\mu \sin(p_\mu a)}{\sum_{\mu=1}^{4}\gamma_\mu \sin^2(p_\mu a)} \tag{2.33}$$

implies that there are fifteen unphysical poles in addition to a physical pole. Particles corresponding to these extra poles are called doublers and we need to remove them to get physically meaningful results on a lattice.

2.2.2 One solution for doubling problem

One solution for the doubling problem in case of free theory is to add the extra term D^W_{free} which has no contribution in the continuum limit to the Dirac operator D as follows;

$$D^W_{free}(n|m) = -\frac{r}{2a}\sum_{\mu=1}^{4}\Big(\delta_{n+\hat{\mu},m} - 2\delta_{nm} + \delta_{n-\hat{\mu},m}\Big). \tag{2.34}$$

This method was introduced by Wilson for the first time [55, 56]. Thus, the extra term is called the Wilson term and r is called the Wilson parameter. In

the continuum limit, this term corresponds to $-\frac{ar}{2}\sum_\mu \partial_\mu\partial_\mu\delta_{nm}$. This Wilson term can be generalized for interacting case considering the invariance under the gauge transformation discussed in previous section as follows;

$$D^W(n|m) = -\frac{r}{2a}\sum_{\mu=1}^{4}\Big(U_\mu(n)\delta_{n+\hat{\mu},m} - 2\delta_{nm} + U_{-\mu}(n)\delta_{n-\hat{\mu},m}\Big). \tag{2.35}$$

Therefore, the Dirac operator D^{WF} for interaction case with Wilson term is given by

$$\begin{aligned} D^{WF}(n|m)^{cd}_{\alpha\beta} &= \sum_{\mu=1}^{4}(\gamma_\mu)_{\alpha\beta}\frac{U_\mu(n)^{cd}\delta_{n+\hat{\mu},m} - U_{-\mu}(n)^{cd}\delta_{n-\hat{\mu},m}}{2a} + m\delta_{\alpha\beta}\delta^{cd}\delta_{nm} \\ &\quad - \frac{r}{2a}\sum_{\mu=1}^{4}\Big(\delta_{n+\hat{\mu},m} - 2\delta_{nm} + \delta_{n-\hat{\mu},m}\Big)\delta^{cd}\delta_{\alpha\beta} \\ &= \left(m + \frac{4r}{a}\right)\delta^{cd}\delta_{\alpha\beta}\delta_{nm} - \frac{1}{2a}\sum_{\mu=\pm1}^{\pm4}(r-\gamma_\mu)_{\alpha\beta}U^{cd}_\mu(n)\delta_{n+\hat{\mu},m}. \end{aligned} \tag{2.36}$$

For this case, the free Dirac operator in momentum space can be obtained as follows;

$$\tilde{D}^{WF}(p) = m + \frac{1}{a}\sum_{\mu=1}^{4}\Big(1-\cos(p_\mu a)\Big) + \frac{i}{a}\sum_{\mu=1}^{4}\gamma_\mu\sin(p_\mu a). \tag{2.37}$$

From this expression, we can find that the mass of the particle whose momentum is $p = (0,0,0,0)$ is m and the Wilson term has no mass contribution to this particle. In addition, it can be said that masses of doublers are proportional to $1/a$ thanks to $\cos(p_\mu a)$ which comes from the Wilson term. Thus, masses of all doublers are heavy enough to have no contribution to the theory in case of a fine lattice, namely in case of a small enough lattice spacing. Consequently, the physical particle we are interested in can survive and doublers cannot exist in our system in the Wilson fermion formalism. In my work, I adopt this Wilson fermions as fermions on a lattice and the Wilson parameter r is set to 1 as we usually do so for simplicity. In principle, r can be set to any value expect 0. Accordingly, the fermion action used in

my work can be written as

$$D^{WF}(n|m) = \left(m + \frac{4}{a}\right)\delta_{nm} - \frac{1}{2a}\sum_{\mu=\pm1}^{\pm4}(1-\gamma_\mu)U_\mu(n)\delta_{n+\hat{\mu},m}. \tag{2.38}$$

2.3 Improvement of QCD action on a lattice

When we construct the effective QCD action on a lattice, we need to discretize the derivatives included in the continuum action and the discretized errors for the fermion action and the gauge action are $O(a)$ and $O(a^2)$, respectively. Taking a continuum limit, the result is free from this discretized error. However, this is a tough work because we need to adopt a larger lattice to keep the lattice volume constant in the case with a smaller lattice spacing. Therefore, it is reasonable to reduce the statistical error originating from the discretization adding extra terms to a lattice action because the lattice action is not unique.

$O(a)$–improved Wilson fermion action

Let us consider $O(a)$–improvement of the Wilson fermion action S_{eff} defined as

$$S_{\text{eff}} = \int dx^4 \left(T^{(0)} + aT^{(1)}\right). \tag{2.39}$$

$T^{(0)}$ is the usual Lagrangian of the Wilson fermions. To achieve this improvement, we simply need to deal with the following quantities;

$$T_1^{(1)} = \bar{\psi}\sigma_{\mu\nu}F_{\mu\nu}\psi, \tag{2.40}$$

$$T_2^{(1)} = \bar{\psi}D_\mu D_\mu\psi + \bar{\psi}\tilde{D}_\mu\tilde{D}_\mu\psi, \tag{2.41}$$

$$T_3^{(1)} = m\mathrm{Tr}[F_{\mu\nu}F_{\mu\nu}], \tag{2.42}$$

$$T_4^{(1)} = m\left[\bar{\psi}\gamma_\mu D_\mu\psi - \bar{\psi}\gamma_\mu\tilde{D}_\mu\psi\right], \tag{2.43}$$

$$T_5^{(1)} = m^2\bar{\psi}\psi. \tag{2.44}$$

The tilde on the operator D_μ in above definitions indicates that the operator works on a field on the left–hand side of the operator. Using the equation $(\gamma_\mu D_\mu + m)\psi = 0$ for these candidates, we can obtain the following relations;

$$T_1^{(1)} - T_2^{(1)} + 2T_5^{(1)} = 0, \tag{2.45}$$

$$T_4^{(1)} + 2T_5^{(1)} = 0. \tag{2.46}$$

These relations can be used to eliminate $T_2^{(1)}$ and $T_4^{(1)}$ from these candidates. Therefore, we have only to consider $T_1^{(1)}$, $T_3^{(1)}$, and $T_5^{(1)}$. However, $T_3^{(1)}$ and $T_5^{(1)}$ are already included in the naively discretized QCD action. Thus, only $T_1^{(1)}$ should be included as an extra term to reduce $O(a)$ discretization error and we reach the following improved action S_I^{WF} for the Wilson fermions;

$$S_I^{WF} = S^{WF} + \frac{1}{2} C_{SW} a^5 \sum_n \sum_{\mu<\nu} \bar{\psi}(n) \sigma_{\mu\nu} F_{\mu\nu}(n) \psi(n). \tag{2.47}$$

The real coefficient C_{SW} is called the Sheikholeslami–Wohlert coefficient [66]. $F_{\mu\nu}$ in this improved action is a discretized version of a field strength and the choice is not unique. In this work, the choice

$$F_{\mu\nu}(n) = \frac{-i}{8a^2} \left[Q_{\mu\nu}(n) - Q_{\nu\mu}(n) \right] \tag{2.48}$$

is adopted with

$$Q_{\mu\nu}(n) = U_{\mu,\nu}(n) + U_{\nu,-\mu}(n) + U_{-\mu,-\nu}(n) + U_{-\nu,\mu}(n). \tag{2.49}$$

$O(a^2)$–improved gauge action

For the standard Wilson gauge action which consists of only plaquettes, we can add extra terms which consist of loops with six link variables to reduce the $O(a^2)$ discretization error. The improved gauge action S_I^g can be expressed as follows;

$$S_I^g = c_0(g_0^2)\mathrm{Tr}P + a^2 c_1(g_0^2)\mathrm{Tr}R + a^2 c_2(g_0^2)\mathrm{Tr}C + a^2 c_3(g_0^2)\mathrm{Tr}L. \tag{2.50}$$

P, R, C, and L correspond to the simple plaquette loop, the rectangle loop, the chair–type loop, and the three–dimensional loop in Fig.2.4, respectively. Note that these loops become zero in the continuum limit. Because the link variable U_μ can be written as $U_\mu = \exp[iaA_\mu(n)]$, the action also can be written with the gauge field A_μ. Imposing that the action (2.50) can be expressed as

$$S_g = -\frac{1}{4} \int d^4x F_{\mu\nu}^a F_{\mu\nu}^a \tag{2.51}$$

in the naive continuum limit, we reach the relation

$$c_0 + 8c_1 + 16c_2 + 8c_3 = 1 \tag{2.52}$$

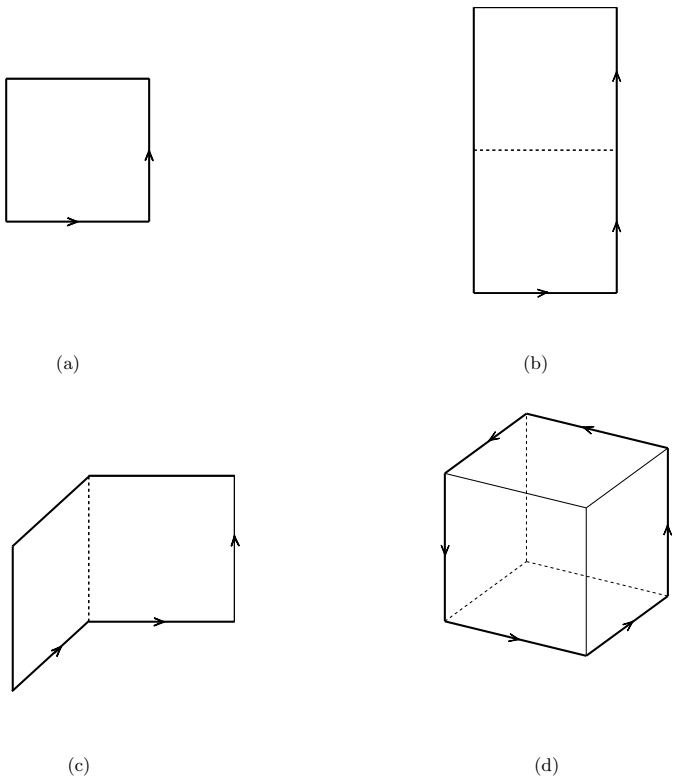

Figure 2.4: Four types of loops included in the improved gauge action. This figure is taken from [65]. (a), (b), (c), and (d) are called a simple plaquette loop, a rectangle loop, a chair–type loop, and a three–dimensional loop.

among the coefficients c_0, c_1, c_2, and c_3. Because c_2 and c_3 can be neglected at the one–loop level, the terms associated with the chair–type loop and the three–dimensional loop are usually dropped and the improved gauge action is given as follows with effective coupling constant $\beta = 6/g^2$ defined by the gauge coupling constant g for $SU(3)$ case.

$$S_{gauge} = \frac{\beta}{3}\Big[(1-8c_1)\sum_{n,\mu<\nu}\mathrm{Tr}P_{\mu,\nu}(n) + c_1\sum_{n,\mu<\nu}\mathrm{Tr}R_{\mu,\nu}\Big], \tag{2.53}$$

$$P_{\mu,\nu} = U_\mu(n)U_\nu(n+\hat{\mu})U_\mu^\dagger(n+\hat{\nu})U_\nu^\dagger(n), \tag{2.54}$$

$$R_{\mu,\nu}(n) = U_\mu(n)U_\mu(n+\hat{\mu})U_\nu^\dagger(n+2\hat{\mu})U_\mu^\dagger(n+\hat{\mu}+\hat{\nu})U_\mu^\dagger(n+\hat{\mu})U_\nu^\dagger(n), \tag{2.55}$$

The improved gauge action with the coefficient $c_1 = -0.331$ are called Iwasaki gauge action and the estimation of the coefficient is based on the renormalization group approach [65].

Chapter 3

Finite temperature and density QCD on a lattice

In this chapter, a method for introducing at finite temperature and density on a lattice is shortly explained. In an actual calculation of lattice QCD, Monte Carlo method needs to be used to obtain an expectation value of an observable. However, at finite density lattice QCD, Monte Carlo method breaks down because the probability density used for Monte Carlo integration becomes complex in general. This problem is called the sign problem. The sign problem is discussed from the point of view of not only the continuum theory but also the discretized one.

3.1 QCD partition function and introduction of temperature and quark chemical potential

According to statistical mechanics with path integral quantization in imaginary time, the QCD grand canonical partition function $Z_{GC}(T, \mu_q)$ at finite temperature T and finite quark chemical potential (corresponding to finite

density) μ_q can be given as

$$\begin{aligned} Z_{GC}(T,\mu_q) &= \mathrm{tr}\Big(e^{-\frac{1}{T}(\hat{H}-\mu_q\hat{N})}\Big) \\ &= \int DU D\bar{\psi}D\psi \exp\left[-\int_0^{\frac{1}{T}} dt \int d^3x\, \bar{\psi}(x)D(\mu_q)\psi(x) - S_{\mathrm{gauge}}\right] \\ &= \int DU \det D(\mu_q)\, e^{-S_{\mathrm{gauge}}}, \end{aligned} \tag{3.1}$$

where D is the Dirac operator at vanishing density discussed in the previous chapter and $D(\mu_q) = D + \mu_q\gamma_4$ for the simplicity. Note that the interval of the integration in the time direction becomes finite and temperature should appear in the upper limit as $1/T$ in the finite temperature theory in contrast with the theory at zero temperature. Therefore, temperature can be introduced on a lattice in the following manner;

$$N_t a = \frac{1}{T}. \tag{3.2}$$

Moreover, we should pay attention to the following anti–periodic boundary condition for the quark fields;

$$\psi(\vec{x}, 1/T) = -\psi(\vec{x}, 0). \tag{3.3}$$

This condition can be checked considering the thermal two point correlation function $G(\vec{x},\vec{y};t,0)$ defined as follows;

$$G(\vec{x},\vec{y};t,0) = \frac{\mathrm{tr}\Big(e^{-(\hat{H}-\mu_q\hat{N})/T}\hat{\psi}(\vec{x},t)\hat{\psi}(\vec{y},0)\Big)}{Z_{GC}(T,\mu_q)}. \tag{3.4}$$

Using the cyclic property of a trace and the anti–commutation relation for fermion fields, this function can be rewritten as

$$\begin{aligned} G(\vec{x},\vec{y};t,0) &= \frac{\mathrm{tr}\Big(e^{-(\hat{H}-\mu_q\hat{N})/T}\hat{\psi}(\vec{x},t)\hat{\psi}(\vec{y},0)\Big)}{Z_{GC}} \\ &= \frac{\mathrm{tr}\Big(e^{-(\hat{H}-\mu_q\hat{N})/T}e^{(\hat{H}-\mu_q\hat{N})/T}\hat{\psi}(\vec{y},0)e^{-(\hat{H}-\mu_q\hat{N})/T}\hat{\psi}(\vec{x},t)\Big)}{Z_{GC}} \\ &= \frac{\mathrm{tr}\Big(e^{-(\hat{H}-\mu_q\hat{N})/T}\hat{\psi}(\vec{y},1/T)\hat{\psi}(\vec{x},t)\Big)}{Z_{GC}} \\ &= -G(\vec{x},\vec{y};t,1/T). \end{aligned} \tag{3.5}$$

This relation exactly implies the condition (3.3).

Next, let us consider how to introduce the quark chemical potential on a lattice. Introducing the quark chemical potential, Lagrangian of interacting quarks should be changed as follows;

$$\bar{\psi}\Big[\gamma_\mu(\partial_\mu + iA_\mu) + m\Big]\psi \to \bar{\psi}\Big[\gamma_\mu(\partial_\mu + iA_\mu) + m - \mu_q A_4\Big]\psi. \tag{3.6}$$

This simply implies that the chemical potential can be introduced by the replacement $A_4 \to A_4 - i\mu_q$. Consequently, the quark chemical potential can be introduced on a lattice by the replacement

$$U_4 = e^{iaA_4} \to e^{ia(A_4 - i\mu_q)} = e^{\mu_q a} U_4 \tag{3.7}$$

for link variables in the time direction [57]. Therefore, the Dirac operator for Wilson fermions at finite chemical potential can be given as

$$\begin{aligned} D^{WF}(n|m;\mu)^{cd}_{\alpha\beta} = &\left(m + \frac{4}{a}\right)\delta^{cd}\delta_{\alpha\beta}\delta_{nm} \\ &- \frac{1}{2a}\sum_{i=\pm1}^{\pm3}(1-\gamma_i)_{\alpha\beta}U_i^{cd}(n)\delta_{n+\hat{i},m} \\ &- \frac{1}{2a}(1-\gamma_4)_{\alpha\beta}\, e^{\mu_q a}U_4^{cd}(n)\delta_{n+\hat{4},m} \\ &- \frac{1}{2a}(1+\gamma_4)_{\alpha\beta}\, e^{-\mu_q a}U_{-4}^{cd}(n)\delta_{n-\hat{4},m}. \end{aligned} \tag{3.8}$$

Note that the Wilson gauge action is invariant under this replacement (3.7) because it consists of plaquettes. Just in case, let us check if this Dirac operator at finite density on a lattice can reproduce the continuum Dirac operator at finite density in the continuum limit. For this check, we have

only to consider the continuum limit of the last two terms of Eq.(3.8);

$$
\begin{aligned}
&-\frac{1}{2a}\sum_n \bar{\psi}(n)\Big[(1-\gamma_4)\, e^{\mu_q a} U_4(n)\psi(n+\hat{4}) + (1+\gamma_4)\, e^{-\mu_q a} U_{-4}(n)\psi(n-\hat{4})\Big] \\
&= -\frac{1}{2a}\sum_n \bar{\psi}(n)\Big[(1-\gamma_4)\, U_4(n)\psi(n+\hat{4}) + (1+\gamma_4)\, U_{-4}(n)\psi(n-\hat{4})\Big] \\
&\quad -\frac{1}{2}\sum_n \bar{\psi}(n)\Big[(1-\gamma_4)\,\mu_q\psi(n) - (1+\gamma_4)\,\mu_q\psi(n) + O(a)\Big] \\
&= -\frac{1}{2a}\sum_n \bar{\psi}(n)\Big[(1-\gamma_4)\, U_4(n)\psi(n+\hat{4}) + (1+\gamma_4)\, U_{-4}(n)\psi(n-\hat{4})\Big] \\
&\qquad\qquad + \sum_n \mu_q \bar{\psi}(n)\gamma_4\psi(n) + O(a). \qquad (3.9)
\end{aligned}
$$

Therefore, the last line corresponds to the term with the quark chemical potential in the continuum theory when taking the continuum limit.

In numerical calculation, we cannot handle quantities which have physical dimension. Thus, the Dirac operator of (3.8) cannot be on a computer. To avoid this problem, we usually adopt the following redefinition of quark fields;

$$
\psi \to \psi' = \sqrt{m + \frac{4}{a}}\,\psi. \qquad (3.10)
$$

Then, we can reach the following dimensionless Dirac operator for Wilson fermions;

$$
\begin{aligned}
D^{WF}(n|m;\mu)^{ab}_{\alpha\beta} &= \delta^{ab}\delta_{\alpha\beta}\delta_{nm} - \kappa\sum_{i=\pm1}^{\pm3}(1-\gamma_i)_{\alpha\beta} U_i^{ab}(n)\delta_{n+\hat{i},m} \\
&\quad - \kappa(1-\gamma_4)_{\alpha\beta}\, e^{\mu_q a} U_4^{ab}(n)\delta_{n+\hat{4},m} \\
&\quad - \kappa(1+\gamma_4)_{\alpha\beta}\, e^{-\mu_q a} U_{-4}^{ab}(n)\delta_{n-\hat{4},m}, \qquad (3.11)
\end{aligned}
$$

where

$$
\kappa = \frac{1}{2ma+8}. \qquad (3.12)
$$

Note that the quark mass can be tuned by the value of κ in actual numerical computations. In the following from here, D^{WF} means this dimensionless Dirac operator on a lattice.

3.2 Lattice QCD and Monte Carlo method

Now, let us consider how to calculate the grand canonical partition function (3.1) on a lattice. If we can get the QCD grand canonical partition function at finite density, we can easily calculate dimensionless thermodynamic observables such as the pressure p, the number density n and the susceptibility χ at finite density as follows;

$$\begin{aligned}\frac{\Delta p(\mu_q,T)}{T^4} &= \frac{p(\mu_q,T)}{T^4} - \frac{p(0,T)}{T^4} \\ &= \left(\frac{N_t}{N_x N_y N_y}\right)^3 \log\left(\frac{Z_{GC}(\mu_q,T)}{Z_{GC}(0,T)}\right),\end{aligned} \tag{3.13}$$

$$\frac{n(\mu_q,T)}{T^3} = \frac{\partial}{\partial(\mu_q/T)}\frac{\Delta p(\mu_q,T)}{T^4}, \tag{3.14}$$

$$\frac{\chi(\mu_q,T)}{T^2} = \frac{\partial^2}{\partial(\mu_q/T)^2}\frac{\Delta p(\mu_q,T)}{T^4}. \tag{3.15}$$

The path integral representation of the grand canonical partition function can be written apparently as follows;

$$\begin{aligned}Z_{GC}(T,\mu_q) &= \int DU \det D(\mu_q)\, e^{-S_{\text{gauge}}} \\ &= \int \prod_{x_1=1}^{N_x}\prod_{x_2=1}^{N_y}\prod_{x_3=1}^{N_z}\prod_{x_4=1}^{N_t}\prod_{\mu=1}^{4} dU_\mu(x_1,x_2,x_3,x_4) \det D(\mu_q)\, e^{-S_{\text{gauge}}}.\end{aligned} \tag{3.16}$$

In QCD, link variables U_μ can be represented by eight parameters with the eight generators for $SU(3)$. The number of dimensions of the integral is $N_{dim} = 8 \times 4 \times N_x \times N_y \times N_z \times N_t$ and this is a highly multiple integral. Therefore, it is not realistic for us to estimate the integral using a quadrature by parts. In an actual calculation, we evaluate the integral making use of Monte Carlo integration with importance sampling. For this strategy, the grand canonical partition function can be rewritten in the following expres-

sion as a most naive way;

$$\begin{aligned} Z_{GC}(T,\mu_q) &= \int DU \det D(\mu_q)\, e^{-S_{\text{gauge}}} \\ &= \int DU \left[\frac{\det D(\mu_q)}{\det D(\mu_0)}\right] \det D(\mu_0)\, e^{-S_{\text{gauge}}} \\ &\equiv \int DU \left[\frac{\det D(\mu_q)}{\det D(\mu_0)}\right] P(U,\mu_0). \end{aligned} \tag{3.17}$$

The most important point of this rewriting is that we regard $P(U,\mu_0)$ as the probability density (Boltzmann weight). Making use of this interpretation, we can generate suitable sets of link variables according to the probability density $P(U,\mu_0)$. Then, we calculate the grand canonical partition function as the statistical average of the ratio of the determinant using the sets of link variables as follows;

$$Z_{GC}(T,\mu_q) = \lim_{N\to\infty} \frac{1}{N} \sum_{i=1}^{N} \frac{\det D(\mu_q, U^i)}{\det D(\mu_0, U^i)}. \tag{3.18}$$

The remaining problem is how to choose μ_0 for the probability density $P(U,\mu_0)$. To come right to the point, μ_0 can be set to 0 or purely imaginary value. This is because $P(U,\mu_0)$ has complex value for real value of μ_0 and we cannot handle $P(U,\mu_0)$ as the probability density in this case. If μ_q is small enough, we can calculate the grand canonical partition function at the chemical potential using Monte Carlo integration according to the $P(U,\mu_0)$ at $\mu_0 = 0$ or purely imaginary valued μ_0. However, we can no longer evaluate the grand canonical partition function at a large quark chemical potential because $P(U,\mu_0)$ at $\mu_0 = 0$ or purely imaginary valued μ_0 is not suitable probability density for the large μ_q case. This problem is called the overlap problem. That is, at finite density QCD, it is important to weaken the overlap problem.

3.3 Sign problem at finite density QCD

3.3.1 Sign problem

In this section, let us consider the sign problem [4, 42, 43] in view of the eigenvalues of the Dirac operator in the continuum theory. As stated previously,

the Dirac operator at finite density is given by

$$D(\mu_q) = D_\mu \gamma_\mu + m + \mu_q \gamma_4. \tag{3.19}$$

Case at vanishing density

In this case, the Dirac operator is

$$D(0) = D_\mu \gamma_\mu + m \tag{3.20}$$

and we can easily find that this operator is anti–hermitian

$$D(0) = -D^\dagger(0). \tag{3.21}$$

Therefore, the eigenvalues of the Dirac operator are purely imaginary;

$$D(0)\psi_i = i\xi_i \psi_i, \tag{3.22}$$

where ψ_i is the eigenstate of the Dirac operator and the eigenvalue $\xi_i \in \mathbb{R}$. Using the anti–commutation relation between γ_5 and γ_μ

$$\{\gamma_5, \gamma_\mu\} = 0, \tag{3.23}$$

we can say that $\gamma_5 \psi_i$ is also the eigenstate of the Dirac operator satisfying

$$D(0)\gamma_5 \psi_i = -i\xi_i \gamma_5 \psi_i. \tag{3.24}$$

Consequently, we can calculate the determinant of the Dirac operator for these sets of the eigenstates as follows;

$$\begin{aligned} \det D(0) &= \prod_n (i\xi_n + m)(-i\xi_n + m) \\ &= \prod_n \left(\xi_n^2 + m^2\right). \end{aligned} \tag{3.25}$$

This means that the determinant always has a real value and the probability density $P(U, 0)$ for Monte Carlo integration is real at vanishing density. Thus, we can conclude that Monte Carlo method can work for the case at vanishing density.

Case at finite density

In contrast to the case at vanishing density, the Dirac operator at finite density is no longer anti–hermitian;

$$D^\dagger(\mu_q) = -D_\mu\gamma_\mu + m + \mu_q\gamma_4. \tag{3.26}$$

Accordingly, the eigenvalues are generally complex as follows;

$$D(\mu_q)\psi_i = \lambda_i\psi_i, \tag{3.27}$$

$$D(\mu_q)\gamma_5\psi_i = -\lambda_i\gamma_5\psi_i, \tag{3.28}$$

where $\lambda_i \in \mathbb{C}$. Therefore, we obtain

$$\begin{aligned}\det D(\mu_q) &= \prod_n (\lambda_n + m)(-\lambda_n + m) \\ &= \prod_n (-\lambda_n^2 + m^2).\end{aligned} \tag{3.29}$$

In this case the determinant is complex in general and the corresponding probability density $P(U, \mu_q)$ becomes complex. Thus, we cannot regard $P(U, \mu_q)$ as the probability density and Monte Carlo method breaks down.

Case at purely imaginary chemical potential

From above discussion, we can say that the probability density becomes real in case of purely imaginary chemical potential $\mu_q = i\mu_I$. This is because the corresponding Dirac operator is anti–hermitian for this case;

$$D(\mu_q = i\mu_I) = -D^\dagger(\mu_q = i\mu_I). \tag{3.30}$$

Thus, the purely imaginary chemical potential is sometimes used for the calculation of an expectation value of an observable at finite density. In usual attempts with purely imaginary chemical potential for finite density QCD, expectation values are calculated in purely imaginary chemical potential region at first and then the results are extrapolated to real chemical potential region by analytic continuation using a polynomial of the chemical potential squared. This method is explained in the next chapter more precisely.

3.3.2 Interpretation of sign problem in view of lattice field theory

In this section, let us consider the sign problem in view of field theory on a lattice. In order to consider the physical interpretation of each term in the Dirac operator, let us rewrite the Dirac operator as follows;

$$\begin{aligned} D^{WF}(n|m;\mu)^{ab}_{\alpha\beta} =& \delta^{ab}\delta_{\alpha\beta}\delta_{nm} - \kappa\sum_{i=\pm1}^{\pm3}(1-\gamma_i)_{\alpha\beta}U_i^{ab}(n)\delta_{n+\hat{i},m} \\ & - \kappa(1-\gamma_4)_{\alpha\beta}\, e^{\mu_q a}U_4^{ab}(n)\delta_{n+\hat{4},m} \\ & - \kappa(1+\gamma_4)_{\alpha\beta}\, e^{-\mu_q a}U_{-4}^{ab}(n)\delta_{n-\hat{4},m} \\ =& 1-\kappa Q(\mu_q). \end{aligned} \tag{3.31}$$

Using this expression, we can obtain the quark propagator D^{-1} in the following way by the expansion in terms of κ;

$$D^{-1} = \frac{1}{1-\kappa Q(\mu_q)} = \sum_{n=1}^{\infty}\Big(\kappa Q(\mu_q)\Big)^n. \tag{3.32}$$

From this expansion, we can find that $Q(\mu_q)$ denotes the quark hopping; the term including $\delta_{n\pm\hat{\mu},m}$ denotes the quark hopping from n to $n\pm\hat{\mu}$. Note that the hopping $n\to n\pm\hat{\mu}\to n$ is excluded because the product $(1\mp\gamma_\mu)(1\pm\gamma_\mu)$ is included in Dirac space for this quark hopping and this product always becomes zero. It also can be found that κ means the mobility of quarks as this parameter depends on the quark mass. This parameter is usually called a hopping parameter. Using this hopping parameter expansion, we can calculate the logarithm of fermion determinant as follows;

$$\begin{aligned} \log\det D^{WF}(\mu_q) = \log\det D^{WF}(\mu_q) &= \mathrm{Tr}\log\Big(1-\kappa Q(\mu_q)\Big) \\ &= -\sum_{l=1}^{\infty}\mathrm{Tr}\frac{\kappa^l Q^n(\mu_q)}{l}. \end{aligned} \tag{3.33}$$

We can choose a basis vector characterized by spacetime (n), Dirac (μ) and color (a) indices for the calculation of the trace. Therefore, we can reach the following expression;

$$\log\det D^{WF}(\mu_q) = -\sum_{a,\mu,n}\sum_{l=1}^{\infty}\left\langle a,\mu,n\right|Q^l(\mu_q)\left|a,\mu,n\right\rangle. \tag{3.34}$$

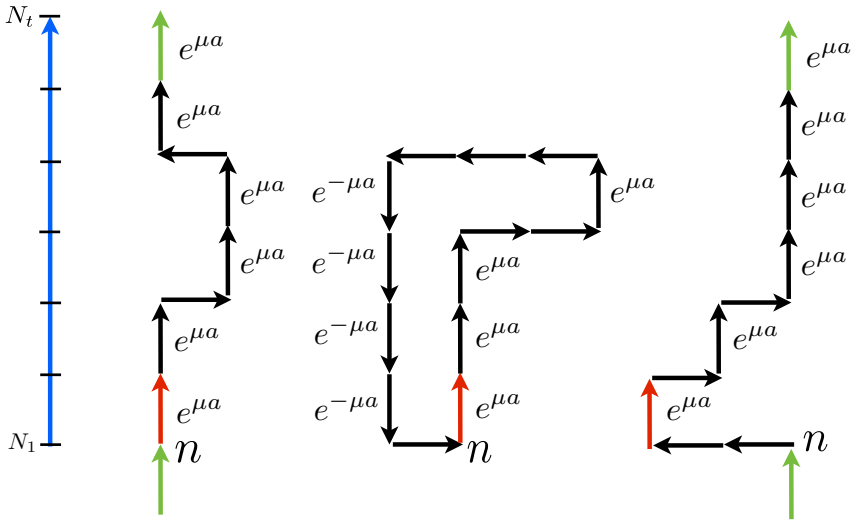

Figure 3.1: Some examples of closed loops starting from n on a lattice. A red arrow denotes a quark hopping starting from a point n and a green arrow denotes the quark hopping coming through anti–periodic boundary condition in the time direction. Closed loops on the right and left hand side are winding around time direction through an anti–periodic boundary condition and this type of closed loops only have a chemical potential dependence. In contrast to these loops, the closed loop in the middle has no chemical potential dependence.

From this expression, we can find that quark hoppings from n to n only have non–zero contribution to this summation. Namely, this type of the quark hoppings form a variety of closed loops on a lattice. Moreover, we can say that the closed loops winding around time direction through anti–periodic boundary condition only have a chemical potential dependence. Consequently, we can rewrite the expansion of the logarithm of the fermion determinant using sets of complex constants C_n and C_{-n} in the following expression [47, 49];

$$\log\det D^{WF}(\mu_q) = C_0 + \sum_{n=1}^{\infty}\left\{C_n e^{n\mu_q/T} + C_{-n}e^{-n\mu_q/T}\right\}. \tag{3.35}$$

Here, n denotes a number of windings around the time direction.

Chapter 4

Canonical approach and other methods to finite density lattice QCD

In this chapter, several methods frequently used for finite density lattice QCD are shortly introduced with the explanation about the difficulties. After that, basic concepts of the canonical approach are introduced [44, 45, 46, 47, 48, 49]. The canonical partition functions correspond to coefficients of the fugacity expansion of the grand canonical partition function. The canonical approach is free from the sign problem in principle because the canonical partition functions are given by the Fourier transformation of the grand canonical partition functions calculated at purely imaginary quark chemical potential.

4.1 Several methods for finite density lattice QCD

In this section, the multi–parameter reweighting method [22, 33], the Taylor expansion method [34, 35, 36], the imaginary chemical potential method [37, 38], and the density of states method [39, 40, 41] which are used to analyze finite density QCD at a small quark chemical potential are briefly introduced.

4.1.1 Multi–parameter reweighting method

For N_f–flavor QCD case, the grand canonical partition function Z_{GC} at finite quark chemical potential μ_q is given with effective coupling $\beta = 6/g^2$ as follows;

$$Z_{GC}(\mu_q) = \int [dU] \Big[\det D(\mu_q) \Big]^{N_f} e^{-\beta S_{gauge}}. \tag{4.1}$$

In the multi–parameter reweighting approach, this grand canonical partition function identically needs to be rewritten with an artificial parameter β_0 in the following expression;

$$\begin{aligned} Z_{GC}(\mu_q) &= \int [dU] \left[\frac{\det D(\mu_q)}{\det D(0)} \right]^{N_f} e^{-(\beta-\beta_0)S_{gauge}} \Big[\det D(0) \Big]^{N_f} e^{-\beta_0 S_{gauge}} \\ &= \int [dU] R(\mu_q, \beta; 0, \beta_0) \Big[\det D(0) \Big]^{N_f} e^{-\beta_0 S_{gauge}}, \end{aligned} \tag{4.2}$$

where

$$R(\mu_q, \beta; 0, \beta_0) \equiv \left[\frac{\det D(\mu_q)}{\det D(0)} \right]^{N_f} e^{-(\beta-\beta_0)S_{gauge}}. \tag{4.3}$$

An important point of this approach is that gauge configurations are produced according to the probability $P(\beta_0) = [\det D(0)]^{N_f} e^{-\beta_0 S_{gauge}}$ and this procedure does not suffer from the sign problem.

What we have to consider as a next step is how to vary β and μ_q keeping on having suitable contribution from Monte Carlo integration with the probability $P(\beta_0)$. We can obtain an ideal guideline for this trial by considering the minimization process of the dispersion $X(\mu_q, \beta, \beta_0)$ of $R(\mu_q, \beta; 0, \beta_0)$ defined as

$$X(\mu_q, \beta, \beta_0) = \big\langle R^2(\mu_q, \beta; 0, \beta_0) \big\rangle_{\beta_0} - \langle R(\mu_q, \beta; 0, \beta_0) \rangle^2_{\beta_0} \tag{4.4}$$

under the infinitesimal transformation $(\beta, \mu_q) \to (\beta + \Delta\beta, \mu_q + \Delta\mu_q)$. Note that $\langle O \rangle_{\beta_0}$ denotes an expectation value of an operator O as a statistical average over configurations produced according to the probability $P(\beta_0)$. Let us consider the deviation of $X(\mu_q, \beta, \beta_0)$ defined under the infinitesimal transformation as follows;

$$\begin{aligned} \delta X &= X(\mu_q + \Delta\mu_q, \beta + \Delta\beta, \beta_0) - X(\mu_q, \beta, \beta_0) \\ &= \frac{\partial X}{\partial(\mu_q/T)} \frac{\Delta\mu_q}{T} + \frac{\partial X}{\partial \beta} \Delta\beta. \end{aligned} \tag{4.5}$$

From Eq.(4.4), we can get the following expressions;

$$\frac{\partial X}{\partial(\mu_q/T)} =2\left\langle \frac{\partial R}{\partial(\mu_q/T)}R\right\rangle_{\beta_0} - 2\left\langle R\right\rangle_{\beta_0}\left\langle \frac{\partial R}{\partial(\mu_q/T)}\right\rangle_{\beta_0}, \tag{4.6}$$

$$\frac{\partial X}{\partial \beta} =2\left\langle \frac{\partial R}{\partial \beta}R\right\rangle_{\beta_0} - 2\left\langle R\right\rangle_{\beta_0}\left\langle \frac{\partial R}{\partial \beta}\right\rangle_{\beta_0}, \tag{4.7}$$

$$\begin{aligned}\frac{\partial R}{\partial(\mu_q/T)} &= \frac{1}{[\det D(\mu_q)]^{N_f}}\frac{\partial[\det D(\mu_q)]^{N_f}}{\partial(\mu_q/T)}\left[\frac{\det D(\mu_q)}{\det D(0)}\right]^{N_f} e^{-(\beta-\beta_0)S_{gauge}} \\ &= \frac{1}{[\det D(\mu_q)]^{N_f}}\frac{\partial[\det D(\mu_q)]^{N_f}}{\partial(\mu_q/T)}R \\ &\equiv C(\mu_q)R,\end{aligned} \tag{4.8}$$

where

$$\frac{\partial R}{\partial \beta} = -S_{gauge}R. \tag{4.9}$$

Therefore, we can get the following expression;

$$\begin{aligned}\frac{\delta X}{2} =& \left\langle C(\mu_q)R^2(\mu_q,\beta;0,\beta_0)\right\rangle_{\beta_0}\frac{\Delta\mu_q}{T} - \left\langle S_{gauge}R^2(\mu_q,\beta;0,\beta_0)\right\rangle_{\beta_0}\Delta\beta \\ &- \left\langle R(\mu_q,\beta;0,\beta_0)\right\rangle_{\beta_0}\left\langle C(\mu_q)R(\mu_q,\beta;0,\beta_0)\right\rangle_{\beta_0}\frac{\Delta\mu_q}{T} \\ &+ \left\langle R(\mu_q,\beta;0,\beta_0)\right\rangle_{\beta_0}\left\langle S_{gauge}R(\mu_q,\beta;0,\beta_0)\right\rangle_{\beta_0}\Delta\beta.\end{aligned} \tag{4.10}$$

From the minimization condition $\delta X = 0$, we can obtain the following relation between $\Delta\beta$ and $\Delta\mu_q/T$.

$$\frac{T\Delta\beta}{\Delta\mu_q} = \frac{\left\langle C(\mu_q)R^2(\mu_q,\beta;0,\beta_0)\right\rangle_{\beta_0} - \left\langle R(\mu_q,\beta;0,\beta_0)\right\rangle_{\beta_0}\left\langle C(\mu_q)R(\mu_q,\beta;0,\beta_0)\right\rangle_{\beta_0}}{\left\langle S_{gauge}R^2(\mu_q,\beta;0,\beta_0)\right\rangle_{\beta_0} - \left\langle R(\mu_q,\beta;0,\beta_0)\right\rangle_{\beta_0}\left\langle S_{gauge}R(\mu_q,\beta;0,\beta_0)\right\rangle_{\beta_0}} \tag{4.11}$$

Using this relation, we can determine suitable values of $\Delta\mu_q$ and $\Delta\beta$ for the probability $P(\beta_0)$ and perform the multi–parameter reweighting method for finite density lattice QCD.

In this approach, we need to calculate the factor R to get an expectation value of an observable. In the factor R, the fermion determinant $\det D(\mu_q)$ is included. Let us rewrite the fermion determinant as follows;

$$\det D(\mu_q) = |\det D(\mu_q)|e^{i\theta}. \tag{4.12}$$

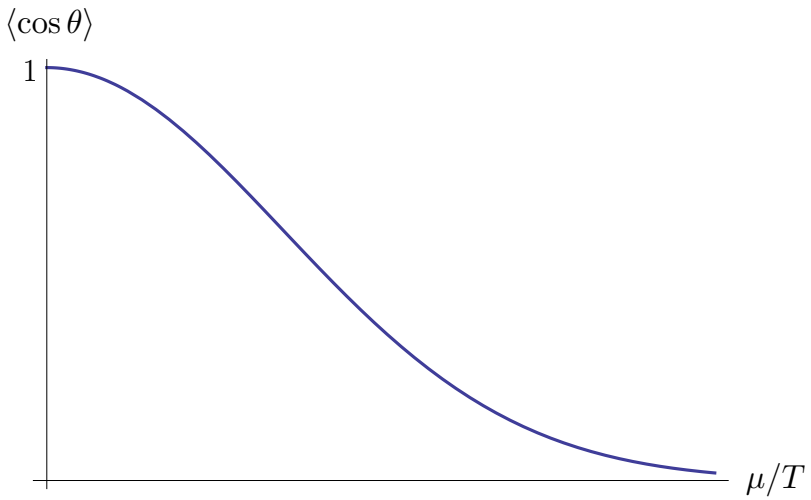

Figure 4.1: Schematical view of the expectation value of θ in fermion determinant against quark chemical potential.

It is known that the expectation value of $\cos\theta$ approaches zero rapidly as a quark chemical potential increases as shown in Fig.4.1 [34]. Therefore, we cannot get an expectation value with high precision at a large quark chemical potential even if we adopt the multi–parameter reweighting method discussed above.

4.1.2 Taylor expansion method

Let us consider to expand the thermodynamic observable in terms of the quark chemical potential μ_q. First, we assume that the pressure can be expand as follows;

$$p(\mu_q, T)/T^4 = \sum_{n=0}^{\infty} C_n \left(\frac{\mu_q}{T}\right)^n. \tag{4.13}$$

Now, let us recall the following two facts. One is that pressure can be obtained from the logarithm of grand canonical partition function $Z_{GC}(\mu_q, T)$. The other is that the grand canonical partition function has the relation

$$Z_{GC}(-\mu_q, T) = Z_{GC}(\mu_q, T) \tag{4.14}$$

because of symmetry of charge conjugation. From these facts, we can reach the following expression for pressure;

$$p(\mu_q, T)/T^4 = \sum_{n=0}^{\infty} C_{2n} \left(\frac{\mu_q}{T}\right)^{2n}. \tag{4.15}$$

The coefficients C_{2n} can be calculated as follows;

$$C_{2n} = \frac{1}{(2n)!} \left(\frac{N_t}{N_s}\right)^3 \frac{\partial^{2n}}{\partial(\mu_q/T)^{2n}} \log Z_{GC}(\mu_q, T)\Big|_{\mu_q/T=0}. \tag{4.16}$$

Note that these coefficients can be calculated by Monte Carlo simulation at vanishing quark chemical potential. Therefore, this method is free from the sign problem. However, this method can work only up to $\mu_q/T \sim 1$ ($\mu_B/T \sim 3$) considering the convergence of the expansion. From the expansion of the pressure, we can also calculate the number density and the susceptibility as follows;

$$n(\mu_q, T)/T^3 = \sum_{n=1}^{\infty} (2n) C_{2n} \left(\frac{\mu_q}{T}\right)^{2n-1}, \tag{4.17}$$

$$\chi(\mu_q, T)/T^2 = \sum_{n=1}^{\infty} (2n-1)(2n) C_{2n} \left(\frac{\mu_q}{T}\right)^{2n-2}. \tag{4.18}$$

4.1.3 Imaginary chemical potential method

If we adopt a purely imaginary chemical potential $\tilde{\mu}_q$, the fermion determinant $\det D(\tilde{\mu}_q)$ in the grand canonical partition function

$$Z_{GC}(\tilde{\mu}_q) = \int [dU] \Big[\det D(\tilde{\mu}_q) \Big]^{N_f} e^{-\beta S_{gauge}} \tag{4.19}$$

is real. Therefore, we can calculate the thermodynamic observables in pure imaginary region and it can be back to a real chemical potential μ_q region by the analytic continuation

$$\langle O(\tilde{\mu}_q) \rangle = \sum_{n=0}^{\infty} c_n \left(\frac{\tilde{\mu}_q}{T}\right)^n \longrightarrow \langle O(\mu_q) \rangle = \sum_{n=0}^{\infty} c_n \left(\frac{-i\mu_q}{T}\right)^n. \tag{4.20}$$

4.1.4 Density of states method

There are several types of a density of states method for finite density lattice QCD according to a choice of quantity for a density of state ρ. Here, the case of a phase θ of the fermion determinant is considered as a basic example. In this case, the density of state can be chosen as follows;

$$\rho(\theta) = \langle \delta(\theta - \theta(U)) \rangle_0 \,. \tag{4.21}$$

$\langle \cdots \rangle_0$ is an expectation value calculated with the link variables U generated according to the phase quenched probability $|\det D(\mu_q)| e^{-S_{gauge}}$. Using this density of state, an expectation value of an observable at a finite quark chemical potential μ_q can be calculated as

$$\langle O(\mu_q) \rangle = \frac{1}{Z} \int d\theta \rho(\theta) e^{i\theta} \langle O \rangle_\theta \,. \tag{4.22}$$

Here, Z and $\langle \cdots \rangle_\theta$ are defined as

$$Z = \int d\theta \rho(\theta) e^{i\theta}, \tag{4.23}$$

where

$$\langle O \rangle_\theta = \frac{1}{\rho(\theta)} \langle O \times \delta(\theta - \theta(U)) \rangle_0 \,. \tag{4.24}$$

Note that these quantities can be calculated by lattice QCD simulation and the difficulty is in the determination of the density of states in this method. Let us consider the difficulty of the phase quenched simulation. For 2–flavor case, the phase quenched fermion determinant corresponds to the simulation at a finite isospin chemical potential ($\mu_q = \mu_I$). That is, the quenched fermion determinant can be expressed as

$$|\det D(\mu_q)|^2 = \det D(\mu_q) \det D(-\mu_q). \tag{4.25}$$

However, in the phase quenched fermion determinant case, it is well known that the exotic phase with pion condensation exists in the region $\mu_q > m_\pi/2$. Because the high precision determination of the density of states are required in this region, the actual validity range of this density of states method is limited to a small value of μ_q/T.

4.2 Canonical approach to finite density QCD

The canonical approach was introduced in [44] for the first time and this section is devoted to review the basic concept of the canonical approach.

4.2.1 How to escape from the sign problem in canonical approach

According to statistical mechanics, the canonical ensemble is a statistical system corresponding to a representation of thermodynamics with temperature T, volume V and number N. In contrast to this ensemble, the grand canonical ensemble is a statistical system of thermodynamics described by T, V and chemical potential μ. An important fact is that thermodynamic functions obtained by both ensembles are related to each other by the Legendre transformation and have equivalent thermodynamic information in the thermodynamics limit. Therefore, it is guaranteed that these ensembles can provide us the same thermodynamic results. This fact is called equivalence of ensembles. Thanks to this equivalency, we can choose a suitable ensemble freely when we consider thermodynamic properties of the system we are interested in.

The grand canonical partition function $Z_{GC}(\mu_q, T)$ is given as

$$Z_{GC}(\mu_q, T) = \mathrm{Tr}\, e^{-(\hat{H}-\mu_q \hat{N})/T}, \tag{4.26}$$

where $\hat{H}$, μ_q , $\hat{N}$ and T correspond to Hamiltonian, a quark chemical potential, a number operator and temperature of the system described by QCD, respectively. If we choose the eigenstate $|n\rangle$ of the number operator $\hat{N}$ which leads to the eigenvalue equation $\hat{N}\,|n\rangle = n\,|n\rangle$ to calculate the trace in Eq.(4.26), the grand canonical partition function can be written by the following polynomial;

$$\begin{aligned} Z_{GC}(\mu_q, T) &= \sum_{n=-\infty}^{\infty} \langle n|\, e^{-(\hat{H}-\mu_q \hat{N})/T}\, |n\rangle \\ &= \sum_{n=-\infty}^{\infty} \langle n|\, e^{-\hat{H}/T}\, |n\rangle\, e^{n\mu_q/T} \\ &= \sum_{n=-\infty}^{\infty} Z_n(T) e^{n\mu_q/T}. \end{aligned} \tag{4.27}$$

To get the second line, the relation $[H, N] = 0$ is used. This $Z_n(T)$ is the canonical partition.f Now, let us consider the grand canonical partition function at a purely imaginary quark chemical potential $\mu_q = i\mu_I$ ($\mu_I \in \mathbb{R}$)

$$Z_{GC}(i\mu_I, T) = \sum_{n=-\infty}^{\infty} Z_n(T) e^{in\mu_I/T}. \tag{4.28}$$

From this relation, we can easily find that the canonical partition function can be calculated by the Fourier transformation of the grand canonical partition function calculated at purely imaginary quark chemical potential;

$$Z_n(T) = \frac{1}{2\pi} \int_0^{2\pi} d\Big(\frac{\mu_I}{T}\Big) Z_{GC}(i\mu_I, T) e^{-in\mu_I/T}. \tag{4.29}$$

As stated in the previous chapter, the canonical approach is free for the sign problem in principle and this is a strong point of the canonical approach. Once we get the grand canonical partition functions at purely imaginary quark chemical potential in the range of 0 to $2\pi i$, we can calculate the canonical partition functions through the Fourier transformation Eq.(4.29). Then, we can reconstruct the grand canonical partition function at any real quark chemical potential considering the fugacity expansion Eq.(4.27).

4.2.2 Constraint on canonical partition functions

To consider the property the canonical partition function should have, let us discuss an introduction of quark chemical potential on a lattice again. In the previous chapter, the fermionic part S_F of QCD action with Wilson fermions is given as follows;

$$S_F = a^4 \sum_{n,m} \bar{\psi}(n) D^{WF}(n|m;\mu) \psi(m),$$

where

$$\begin{aligned} D^{WF}(n|m;\mu_q)^{cd}_{\alpha\beta} =& \delta^{cd}\delta_{\alpha\beta}\delta_{nm} - \kappa \sum_{i=\pm1}^{\pm3} (1-\gamma_i)_{\alpha\beta} U_i^{cd}(n) \delta_{n+\hat{i},m} \\ & - \kappa(1-\gamma_4)_{\alpha\beta}\, e^{\mu_q a} U_4^{cd}(n) \delta_{n+\hat{4},m} \\ & - \kappa(1+\gamma_4)_{\alpha\beta}\, e^{-\mu_q a} U_{-4}^{cd}(n) \delta_{n-\hat{4},m}. \end{aligned}$$

For this action, we introduce the following change of variables [58];

$$\psi(\vec{n}, n_4) \longrightarrow e^{-n_4 \mu a}\, \psi(\vec{n}, n_4), \tag{4.30}$$

$$\bar{\psi}(\vec{n}, n_4) \longrightarrow e^{n_4 \mu a}\, \bar{\psi}(\vec{n}, n_4). \tag{4.31}$$

Under this transformation, the first two terms of (4.30) are not changed. The third term and forth term are transformed as follows.

$n_4 \neq N_t$ or $N_t \neq 1$ case for the third and the forth terms

$$\begin{aligned} & -\kappa(1 \mp \gamma_4) e^{\pm \mu_q a} U_{\pm 4}(\vec{n}, n_4) \delta_{n \pm \hat{4}, m} \\ & \to -\kappa e^{n_4 \mu_q a} (1 \mp \gamma_4) e^{\pm \mu_q a} U_{\pm 4}(\vec{n}, n_4) e^{-(n_4 \pm 1)\mu_q a} \delta_{n \pm \hat{4}, m} \\ & = -\kappa(1 \mp \gamma_4) U_{\pm 4}(\vec{n}, n_4) \delta_{n \pm \hat{4}, m} \end{aligned} \tag{4.32}$$

$n_4 = N_t$ case for the third term

$$\begin{aligned} & -\kappa(1 - \gamma_4) e^{\mu_q a} U_4(\vec{n}, N_t) \delta_{n + \hat{4}, m} \\ & \to -\kappa e^{N_t \mu_q a} (1 - \gamma_4) e^{\mu_q a} U_4(\vec{n}, N_t) e^{-\mu_q a} \delta_{n + \hat{4}, m} \\ & = -\kappa(1 - \gamma_4) e^{N_t \mu_q a} U_4(\vec{n}, N_t) \delta_{n + \hat{4}, m} \\ & = -\kappa(1 - \gamma_4) e^{\mu_q / T} U_4(\vec{n}, N_t) \delta_{n + \hat{4}, m} \end{aligned} \tag{4.33}$$

$n_4 = N_t$ case for the forth term

$$\begin{aligned} & -\kappa(1 + \gamma_4) e^{-\mu_q a} U_{-4}(\vec{n}, N_t) \delta_{n - \hat{4}, m} \\ & \to -\kappa e^{N_t \mu_q a} (1 + \gamma_4) e^{-\mu_q a} U_{-4}(\vec{n}, N_t) e^{-(N_t - 1)\mu_q a} \delta_{n - \hat{4}, m} \\ & = -\kappa(1 + \gamma_4) U_{-4}(\vec{n}, N_t) \delta_{n - \hat{4}, m} \end{aligned} \tag{4.34}$$

$n_4 = 1$ case for the third term

$$\begin{aligned} & -\kappa(1 - \gamma_4) e^{\mu_q a} U_4(\vec{n}, 1) \delta_{n + \hat{4}, m} \\ & \to -\kappa e^{\mu_q a} (1 - \gamma_4) e^{\mu_q a} U_4(\vec{n}, 1) e^{-2\mu_q a} \delta_{n + \hat{4}, m} \\ & = -\kappa(1 - \gamma_4) U_4(\vec{n}, 1) \delta_{n + \hat{4}, m} \end{aligned} \tag{4.35}$$

$n_4 = 1$ case for the forth term

$$\begin{aligned} & -\kappa(1 + \gamma_4) e^{-\mu_q a} U_{-4}(\vec{n}, 1) \delta_{n - \hat{4}, m} \\ & \to -\kappa e^{\mu_q a} (1 + \gamma_4) e^{-\mu_q a} U_{-4}(\vec{n}, 1) e^{-N_t \mu_q a} \delta_{n - \hat{4}, m} \\ & = -\kappa(1 + \gamma_4) e^{-\mu_q / T} U_{-4}(\vec{n}, 1) \delta_{n - \hat{4}, m} \end{aligned} \tag{4.36}$$

From the above, we can say that the quark chemical potential can also be introduced using the replacement

$$U_{\pm 4}(\vec{n}, N_t) \longrightarrow e^{\pm \mu_q / T} U_{\pm 4}(\vec{n}, N_t) \tag{4.37}$$

for the link variables only on the time slice $n_4 = N_t$.

4.2.3 Roberge–Weiss periodicity for grand canonical partition function

In this section, we discuss the periodicity of grand canonical partition function at purely imaginary quark chemical potential which is closely related to Z_3 transformation for link variables. Z_3 group is a center group of $SU(3)$. This means that any element of Z_3 group can commute with any element of $SU(3)$ group. In particular, the elements $\{z\}$ of Z_3 group are given as $z = 1, e^{i2\pi/3}, e^{i4\pi/3}$. Now, let us consider the following grand canonical partition function;

$$Z_{GC}\left(i\mu_I + i\frac{2\pi k}{3}\right) = \int [dU] \det D\left(i\mu_I + i\frac{2\pi k}{3}, U\right) e^{-S_{gauge}[U]}. \tag{4.38}$$

Considering the replacement (4.37) to introduce a finite quark chemical potential, this grand canonical partition function can be rewritten as

$$Z_{GC}\left(i\mu_I + i\frac{2\pi k}{3}\right) = \int [dU] \det D(i\mu_I, U') e^{-S_{gauge}[U]}, \tag{4.39}$$

where

$$U'_i(\vec{n}, n_4) = U_i(\vec{n}, n_4), \tag{4.40}$$

$$U'_4(\vec{n}, n_4) = e^{i\frac{2\pi k}{3}\delta_{n_4, N_t}} U_4(\vec{n}, n_4). \tag{4.41}$$

These new link variables U' can be interpreted as the result of Z_3 transformation of original link variables U only on $n_4 = N_t$ plane. It is obvious that the Wilson gauge action is invariant under this transformation because it consists of the sum of plaquettes. This means that $S_{gauge}[U] = S_{gauge}[U']$. Moreover, Haar measure in path integral representation is also invariant under the Z_3 transformation. Therefore, we can state that the right hand side of

(4.39) is equivalent to $Z_{GC}(i\mu_I)$. Consequently, we can finally find the following periodicity of the grand canonical partition function at purely imaginary chemical potential;

$$Z_{GC}(i\mu_I) = Z_{GC}(i\mu_I + 2\pi i n/3) \ \ (n = 1, 2). \tag{4.42}$$

This periodicity is usually called the Roberge–Weiss periodicity [60]. Using the Roberge–Weiss periodicity, we can rewrite the grand canonical partition function as

$$Z_{GC}(i\mu_I) = \frac{1}{3}\sum_{k=0}^{2} Z_{GC}(i\mu_I + 2\pi i k/3) \tag{4.43}$$

and then, we can obtain the following relation;

$$Z_n(T) = \frac{1}{2\pi}\int_0^{2\pi} d\Big(\frac{\mu_I}{T}\Big) Z_{GC}(i\mu_I) e^{-in\mu_I/T} \times \left[\frac{1 + e^{2\pi i n/3} + e^{4\pi i n/3}}{3}\right]. \tag{4.44}$$

From this relation, the following important constraint on the canonical partition functions is given [60, 61];

$$Z_{n\neq 3k}(T) = 0 \ \ (k \in \mathbb{N}). \tag{4.45}$$

Note that this constraint holds true in both the confining and the deconfining phases. Thus, the grand canonical partition function can be written as

$$Z_{GC}(\mu_B, T) = \sum_{B=-\infty}^{\infty} Z_B(T) e^{B\mu_B/T}, \tag{4.46}$$

where $B \in \mathbb{N}$. Because the quantum number B can be interpreted as a net baryon number, μ_B can be regarded as a baryon chemical potential, which is related to a quark chemical potential as $\mu_B = 3\mu_q$.

Chapter 5

Difficulties of canonical approach to finite density lattice QCD and the solutions

5.1 Multiple precision calculation as a new solution for difficulty of Fourier transformation

As the fugacity expansion of the grand canonical partition function should converge at a real baryon chemical potential, the canonical partition function Z_B must decrease when the absolute value of net baryon number B increases. This means that we have to work with very small values in the Fourier transformation results. This Fourier transformation is difficult from the viewpoint of numerical calculation because it is an oscillatory integral.

In the numerical calculation, the Fourier transformation computed by the discrete Fourier transform (DFT) as

$$Z_B = \frac{1}{N}\sum_{k=0}^{N-1} Z_{GC}\left(i\frac{\mu_I}{T} = i\frac{2\pi k}{N}\right) e^{i\frac{2\pi k}{N}B}, \tag{5.1}$$

where N is the interval number of the DFT. As the DFT is simply a discretized version of the Fourier transform in a continuum theory, the difficulty of the DFT in the canonical approach is caused by the numerical errors, the types of which are classified as rounding error, truncation error, cancellation

of significant digits, and loss of trailing digits. The difficulty of the DFT does not arise from truncation error because the DFT is not an infinite series. Accordingly, it is natural to consider that the instability originates from the cancellation of significant digits.

The cancellation of significant digits occurs in the following type of calculation:

$$\begin{array}{lcl} 1.234567 - 1.234566 & = & 0.000001. \\ \text{(7 significant digits)} & & \text{(1 significant digit)} \end{array} \tag{5.2}$$

In this case, six significant digits are lost.

To reduce the effect of this cancellation, the number of significant digits should be increased. Consider the following calculation with 22 significant digits:

$$\begin{array}{l} 1.234567444444444444444 - 1.234566111111111111111 \\ \text{(22 significant digits)} \\ \qquad = \quad 0.000001333333333333333. \\ \qquad\quad \text{(16 significant digits)} \end{array} \tag{5.3}$$

Although six significant digits are still lost in this calculation, 16 significant digits remain in the final result.

Summarizing the above process, the precision of a calculation result can be retained by increasing the significant digits of the input variables in this way. Therefore, the multiple precision calculation should be needed for the canonical approach. This is a new point of view in the context of the Fourier transformation in the canonical approach.

5.2 Winding number expansion method as a new solution for numerical cost for calculations of Wilson fermion determinants

As stated in the previous section, the canonical partition functions can be calculated by the DFT of the grand canonical partition functions computed at purely imaginary chemical potential. This apparently means that Wilson fermion determinants computed at many different values of purely imaginary chemical potentials must be needed. A standard method to calculate Wilson fermion determinants is to perform LU decomposition of the Wilson fermion

matrix. However, in this case, we need to perform the LU decomposition of matrices whose rank is $12N_xN_yN_zN_t$ for several hundreds of gauge configuration at each chemical potential. Therefore, the LU decomposition method is not realistic even with recent computer resources even in case of a small size lattice.

5.2.1 Reduction formula for Wilson fermion determinant

The most reliable method to overcome the above problem on numerical costs is to adopt a reduction formula for the calculation of Wilson fermion determinant [62, 63, 64]. In this method, the Wilson fermion determinant can be calculated as follows.

The Wilson fermion matrix is given as

$$\begin{aligned} D^{WF}(n|m;\mu_q) = 1 - \kappa \sum_{i=1}^{3} \Big[(r-\gamma_i) U_i(n) \delta_{n+\hat{i},m} + (r+\gamma_i) U_i^\dagger(m) \delta_{n-\hat{i},m} \Big] \\ - \kappa (r-\gamma_4)\, e^{\mu_q a} U_4(n) \delta_{n+\hat{4},m} - \kappa (r+\gamma_4)\, e^{-\mu_q a} U_4^\dagger(m) \delta_{n-\hat{4},m}. \end{aligned} \tag{5.4}$$

Note that the Wilson parameter r is not set to 1 at this stage. In the middle of the process to construct the reduction formula, we take the limit $r \to 1$. For later convenience, we rewrite this Wilson fermion matrix as follow;

$$D^{WF}(n|m;\mu_q) = B(n,m) - 2z^{-1}\kappa r_- V(n,m) - 2z\kappa r_+ V^\dagger(n,m), \tag{5.5}$$

where

$$B(n,m) \equiv 1 - \kappa \sum_{i=1}^{3} \Big[(r-\gamma_i) U_i(n) \delta_{n+\hat{i},m} + (r+\gamma_i) U_i^\dagger(m) \delta_{n-\hat{i},m} \Big], \tag{5.6}$$

$$V(n,m) \equiv U_4(n) \delta_{m,n+\hat{4}}, \tag{5.7}$$

$$V^\dagger(n,m) \equiv U_4^\dagger(m) \delta_{m,n-\hat{4}}, \tag{5.8}$$

$$z \equiv e^{-\mu_q a}, \quad r_\pm \equiv \frac{r \pm \gamma_4}{2}. \tag{5.9}$$

From the definition of B, we can easily find that B is a diagonal matrix in the time–plane.

$$B = \begin{pmatrix} B_1 & 0 & \cdots & 0 \\ 0 & B_2 & & \vdots \\ \vdots & & \ddots & 0 \\ 0 & \cdots & 0 & B_{N_t} \end{pmatrix} \tag{5.10}$$

$$B_i \equiv B(\vec{x}, t_i, \vec{y}, t_i) \tag{5.11}$$

Matrix V can be represented in the time–plane as follows;

$$V = \begin{pmatrix} 0 & U_4(\vec{x}, 1) & 0 & \cdots & 0 \\ \vdots & 0 & U_4(\vec{x}, 2) & & \vdots \\ & & & \ddots & 0 \\ & & & & U_4(\vec{x}, N_t - 1) \\ -U_4(\vec{x}, N_t) & \cdots & & & 0 \end{pmatrix}. \tag{5.12}$$

The negative sign on the $(N_t, 1)$ element of V comes from anti–periodic boundary condition.

As a next step, we consider the matrix P defined as

$$P(n, m) \equiv r_- \delta_{n,m} + r_+ V(n, m) z^{-1}. \tag{5.13}$$

The determinant of this matrix P can be calculated in the following manner;

$$\begin{aligned} \det P &= \det \left(r_-^{N_t} \right) \det \left(1 + (r_-^{-1} r_+)^{N_t} z^{-N_t} U_4(\vec{x}, t) \cdots U_4(\vec{x}, N_t) \right) \\ &= \det \left((r_-)^{N_t} + (r_+)^{N_t} z^{-N_t} U_4(\vec{x}, t) \cdots U_4(\vec{x}, N_t) \right). \end{aligned} \tag{5.14}$$

Note that the determinants on the right hand side are taken with respect to the space indices, the color indices and the Dirac indices. This expression can be obtained from the following formula with regular block matrices A_i and B_i;

$$\begin{aligned} &\det \begin{pmatrix} A_1 & B_1 & 0 & \cdots & 0 \\ \vdots & A_2 & B_2 & & \vdots \\ & & \ddots & \ddots & 0 \\ & & & & B_{n-1} \\ -B_n & \cdots & & & A_n \end{pmatrix} \\ &= \det \left(A_1 \cdots A_n \right) \det \left(1 + (-1)^n A_1^{-1} B_1 \cdots A_n^{-1} B_n \right). \end{aligned} \tag{5.15}$$

This formula can be applied to the calculation of $\det P$ as r_- has its inverse

$$r_-^{-1} = \frac{4}{r^2-1} r_+. \tag{5.16}$$

In Eq.(5.14), we can take the limit $r \to 1$ because inverses of r_- are no longer included. In the following discussion from here, we can set r to 1. To calculate the right hand side of Eq.(5.14) for Dirac indices, let us consider matrices r_+ and r_- in Dirac representation;

$$(r_-)^{N_t} = \begin{pmatrix} 0 & 0 & 0 & 0 \\ 0 & 0 & 0 & 0 \\ 0 & 0 & 1 & 0 \\ 0 & 0 & 0 & 1 \end{pmatrix}, \tag{5.17}$$

$$(r_+)^{N_t} = \begin{pmatrix} 1 & 0 & 0 & 0 \\ 0 & 1 & 0 & 0 \\ 0 & 0 & 0 & 0 \\ 0 & 0 & 0 & 0 \end{pmatrix}. \tag{5.18}$$

Using these matrices, we can get the expression.

$$\det P = \det \Big(z^{-N_t} U_4(\vec{x}, 1) \cdots U_4(\vec{x}, N_t) \Big)^2. \tag{5.19}$$

Note that the determinants on the right hand side are taken with respect to the space indices and the color indices. It is easy to calculate the determinant and the final result is

$$\det P = z^{-6N_x N_y N_z N_t}. \tag{5.20}$$

The next step we should consider is the product of matrices D^{WF} and P and the determinant. We can write down the product $D^{WF}P$ as follows;

$$\begin{aligned} (D^{WF}P)(n,m) &= \sum_l D^{WF}(n,l) P(l,m) \\ &= \Big(B(n,m) r_- - 2\kappa r_+ \delta_{n,m} \Big) \\ &\qquad + \sum_l \Big(B(n,l) r_+ - 2\kappa r_- \delta_{n,l} \Big) V(l,m) z^{-1} \\ &\equiv X_1(n,m) + X_2(n,m). \end{aligned} \tag{5.21}$$

We can easily find that the matrix X_1 is a diagonal matrix in the time–plane;

$$X_1 = \begin{pmatrix} \alpha_1 & & & 0 \\ & \alpha_2 & & \\ & & \ddots & \\ 0 & & & \alpha_{N_t} \end{pmatrix}, \tag{5.22}$$

where

$$(\alpha_i)^{ab}_{\mu\nu}(\vec{n},\vec{m}) \equiv B(\vec{n},i,\vec{m},i)^{ab}_{\mu\sigma}(r_-)_{\sigma\nu} - 2\kappa(r_+)_{\mu\nu}\delta^{ab}\delta_{\vec{n},\vec{m}}. \tag{5.23}$$

On the other hand, the matrix X_2 is not diagonal in the time–plane. However, X_2 has the particular form as follows;

$$X_2 = \begin{pmatrix} 0 & \beta_1 z^{-1} & 0 & \cdots & 0 \\ \vdots & 0 & \beta_2 z^{-1} & & \vdots \\ & & & \ddots & 0 \\ & & & \ddots & \beta_{N_t-1} z^{-1} \\ -\beta_{N_t} z^{-1} & \cdots & & & 0 \end{pmatrix}, \tag{5.24}$$

where

$$(\beta_i)^{ab}_{\mu\nu}(\vec{n},\vec{m}) \equiv B(\vec{n},\vec{m},i)^{ac}_{\mu\sigma}(r_+)_{\sigma\nu}U_4^{cb}(\vec{m},i) - 2\kappa(r_-)_{\mu\nu}U_4^{ab}(\vec{m},i)\delta_{\vec{n},\vec{m}}. \tag{5.25}$$

Therefore, the matrix $D^{WF}P$ can be written as

$$D^{WF}P = \begin{pmatrix} \alpha_1 & \beta_1 z^{-1} & 0 & \cdots & 0 \\ \vdots & \alpha_2 & \beta_2 z^{-1} & & \vdots \\ & & & \ddots & 0 \\ & & & \ddots & \beta_{N_t-1} z^{-1} \\ -\beta_{N_t} z^{-1} & \cdots & & & \alpha_{N_t} \end{pmatrix}. \tag{5.26}$$

The determinant of this matrix can be calculated using Eq.(5.15);

$$\det\left(D^{WF}P\right) = \det\left(\prod_{i=1}^{N_t}\alpha_i\right)\det\left(1+z^{-N_t}Q\right), \tag{5.27}$$

where

$$Q \equiv \prod_{i=1}^{N_t}\alpha_i^{-1}\beta_i. \tag{5.28}$$

Note that the determinants on the right hand side are are taken with respect to the Dirac indices, the space indices and the color indices. Consequently, we can obtain the fermion determinant as follow using Eq.(5.20);

$$\det\left(D^{WF}\right) = \frac{\det\left(D^{WF}P\right)}{\det P} = z^{-6N_xN_yN_zN_t}\det\left(\prod_{i=1}^{N_t}\alpha_i\right)\det\left(z^{N_t}+Q\right). \tag{5.29}$$

The notable fact is that the rank of the matrices α_i and Q is not $N = 4N_cN_xN_yN_zN_t$ but $N_{red} = N/N_t$. This means that the reduction formula makes the computation of the determinant less by $1/N_t^3$. To be more specific, we calculate the determinant according to the following procedure. First of all, we need to calculate the eigenvalues $\{\lambda_n\}$ of the matrix Q. Using the set of eigenvalues, we can get the series

$$z^{-6N_xN_yN_zN_t}\det\left(z^{N_t}+Q\right) = \prod_{n=1}^{N_{red}}\left(\lambda_n + z^{N_t}\right) \equiv \sum_{n=-N_{red}/2}^{N_{red}/2} c_n\xi^n \tag{5.30}$$

in terms of fugacity $\xi = e^{n\mu_q/T}$ with a set of complex constants $\{c_n\}$. Then, we can finally obtain the final result

$$\det D^{WF}(\mu_q) = \det\left(\prod_{i=1}^{N_t}\alpha_i\right)\sum_{n=-N_{red}/2}^{N_{red}/2} c_n e^{n\mu_q/T} = \sum_{n=-N_{red}/2}^{N_{red}/2} C_n e^{n\mu_q/T}, \tag{5.31}$$

where

$$C_n \equiv \det\left(\prod_{i=1}^{N_t}\alpha_i\right)c_n. \tag{5.32}$$

Note that C_n is a complex number which does not depend on a quark chemical potential μ_q. Therefore, if we calculate a set of complex numbers $\{C_n\}$ once for a gauge configuration, we calculate the Wilson fermion determinants at all desired purely imaginary chemical potential using the fugacity expansion without additional computational effort. However, we cannot deal with a large lattice if we adopt this reduction formula for the calculation of Wilson fermion determinant. As explained above, we need to consider the eigenvalue problem of the matrices whose rank is $12N_xN_yN_z$. In this procedure, we need to store the matrices on a computer to compute the eigenvalues. For lager lattice case, we can no longer store them considering

the current computer resources. In addition, the time complexities for the reduction formula can be estimated to $O((N_x N_y N_z)^3 \times N_t)$. This means that we need to develop the method which allows us to perform the calculation of fermion determinants at various values of purely imaginary chemical potentials within more reasonable time if we want to compute on the lattice with more lattice sites. Taking this current situation into consideration, we have decided to develop the winding number expansion base on the hopping parameter expansion to overcome these problems for numerical calculation.

5.2.2 Winding number expansion method

Let us recall again the discussion of the hopping parameter expansion in chapter 2 in detail to obtain the numerical method of the winding number expansion. The logarithm of the Wilson fermion determinant can be calculated as follows;

$$\begin{aligned} \log\det D^{WF}(\mu_q) = \log\det D^{WF}(\mu_q) &= \mathrm{Tr}\log\Big(1-\kappa Q(\mu_q)\Big) \\ &= -\sum_{l=1}^{\infty}\mathrm{Tr}\frac{\kappa^l Q^n(\mu_q)}{l}. \end{aligned} \tag{5.33}$$

Because Q has space–time, Dirac and color indices, we can calculate the trace using a set of basis vectors characterized by the indices as follows;

$$\mathrm{Tr}Q^n = \sum_{n,a,\mu}\langle n,a,\mu|\, Q^n\,|n,a,\mu\rangle\,. \tag{5.34}$$

Moreover, we can rewrite this expression as follows from the discussion in chapter 2;

$$\log\det D^{WF}(\mu_q) = C_0 + \sum_{n=1}^{\infty}\Big\{C_n e^{n\mu_q/T} + C_{-n}e^{-n\mu_q/T}\Big\}. \tag{5.35}$$

Note that n denotes a number of windings of a closed quark hopping loop around the time direction. It is apparent from this expression that we can evaluate the fermion determinants at all desired purely imaginary chemical potentials if we have a set of complex valued constants $\{C_n\}$. Therefore, we can drastically reduce the numerical cost for the calculation of fermion determinants in this case. Moreover, we do not need to keep any matrices

on the computer. Thus, we do not need to consider the problem of main memory on a computer.

Let us consider how to calculate this $\{C_n\}$ numerically. For later convenience, we rewrite the Wilson fermion matrix as follows;

$$D^{WF}(n|m;\mu_q) = 1 - \kappa Q_s(n|m) - \kappa Q_4^{(+)}(n|m;\mu_q) - \kappa Q_4^{(-)}(n|m;\mu_q), \quad (5.36)$$

where

$$Q_s(n|m) = \sum_{i=\pm 1}^{\pm 3} (1-\gamma_i)_{\alpha\beta} U_i^{ab}(n) \delta_{n+\hat{i},m}, \quad (5.37)$$

$$Q_4^{(+)}(n|m;\mu_q) = (1-\gamma_4)\, e^{\mu_q a} U_4(n) \delta_{n+\hat{4},m}, \quad (5.38)$$

$$Q_4^{(-)}(n|m;\mu_q) = (1+\gamma_4)\, e^{-\mu_q a} U_{-4}(n) \delta_{n-\hat{4},m}. \quad (5.39)$$

What we need to consider is how to get a set of complex valued constants $\{C_n\}$ numerically from the following series.

$$\log\det D^{WF}(\mu_q) = -\sum_{n,a,\mu} \langle n,a,\mu| \sum_{l=1}^{\infty} \frac{\kappa^l Q^l(\mu_q)}{l} |n,a,\mu\rangle \quad (5.40)$$

Before considering the method, let us consider how to calculate this trace. This is because, in case of a large lattice, it is apparent that the summation over space–time indices n for the trace is numerically expensive. To overcome this problem, the following noise method is used in our calculation.

We introduce random numbers $\eta^{(r)}$ which satisfy

$$\lim_{N_{noise}\to\infty} \frac{1}{N_{noise}} \sum_{r=1}^{N_{noise}} \left(\eta^{(r)}_{n,a,\mu}\right)^* \eta^{(r)}_{m,b,\nu} = \delta_{nm}\delta_{ab}\delta_{\mu\nu}. \quad (5.41)$$

Using this random number, we can calculate the trace as follows;

$$\mathrm{Tr}Q^l = \lim_{N_{noise}\to\infty} \frac{1}{N_{noise}} \sum_{r=1}^{N_{noise}} \left(\eta^{(r)}\right)^\dagger Q^l \eta^{(r)}. \quad (5.42)$$

The number of noise vectors N_{noise} should be chosen properly for the problem we are interested in. However, N_{noise} might be much less than $4N_cN_xN_yN_zN_t$ in our case because Q is a sparse matrix. Therefore, the noise method could reduce the numerical cost for the trace effectively.

Let us go back to the numerical calculation of $\{C_n\}$. The helpful guidance to evaluate $\{C_n\}$ is the number of quark hoppings in the time direction. The contribution from the trace of any quark loops whose winding number is n can be calculated as $C_n e^{\mu_q/T}$ (in detail, see chapter 2). In an actual numerical calculation, we calculate the product $\kappa^l Q^l \times \eta^{(r)}$ for each noise vector $\eta^{(r)}$ and sort the result in terms of the number of hoppings in the time direction. After that, we consider the summation over noise vectors and this corresponds to the result for one configuration. Because this numerical procedure is not straightforward, let us consider how to perform the calculation on a computer in detail to make our understanding clear.

First of all, we make a noise vector $\eta^{(1)}$. Then, we calculate the quantities

$$X^{(1)}(+1) = \kappa Q_4^{(+)}(\mu_q = 0)\eta^{(1)}, \tag{5.43}$$

$$X^{(1)}(0) = \kappa Q_s \eta^{(1)}, \tag{5.44}$$

$$X^{(1)}(-1) = \kappa Q_4^{(-)}(\mu_q = 0)\eta^{(1)} \tag{5.45}$$

which correspond to the contribution of the leading term of the hopping parameter expansion. The variable n and α in $X^{(n)}(\alpha)$ denote the number of times of the hopping parameter expansion and the total quark hoppings in time direction. Because we now consider the leading term of the hopping parameter, n is 1 and the maximum(minimum) value of α is $+1(-1)$. Note that the operation κQ_s has no contribution for the quark hoppings in the time direction. On the other hand, $\kappa Q_4^{(+)}(\mu_q = 0)$ and $\kappa Q_4^{(-)}(\mu_q = 0)$ have the contribution for one time quark hopping in the positive and the negative time direction. In this procedure, we do not need to consider finite chemical potential case. This is because we have only to evaluate a set of complex valued constants $\{C_n\}$ and $\{C_n\}$ has no chemical potential dependence. After this procedure, these $X^n(\alpha)$ need to be saved on a memory to calculate the trace in Eq.(5.40) as follows;

$$Y(+1) = -X^{(1)}(+1), \tag{5.46}$$

$$Y(0) = -X(0)^{(1)}, \tag{5.47}$$

$$Y(-1) = -X(-1)^{(1)}. \tag{5.48}$$

The next step is the following calculation;

$$X^{(2)}(+2) = \kappa Q_4^{(+)}(\mu_q = 0)X^{(1)}(+1), \tag{5.49}$$

$$X^{(2)}(+1) = \kappa Q_s X^{(1)}(+1) + \kappa Q_4^{(+)}(\mu_q = 0) X^{(1)}(0), \tag{5.50}$$

$$\begin{aligned} X^{(2)}(0) =& \kappa Q_s X^{(1)}(0) + \kappa Q_4^{(-)}(\mu_q = 0) X^{(1)}(+1) \\ &+ \kappa Q_4^{(+)}(\mu_q = 0) X^{(1)}(-1), \end{aligned} \tag{5.51}$$

$$X^{(2)}(-1) = \kappa Q_s X^{(1)}(-1) + \kappa Q_4^{(-)}(\mu_q = 0) X^{(1)}(0), \tag{5.52}$$

$$X^{(2)}(-2) = \kappa Q_4^{(-)}(\mu_q = 0) X^{(1)}(-1). \tag{5.53}$$

This procedure corresponds to the next leading order contribution of the hopping parameter expansion. Then, the array $Y(n)$ needs to be overwritten as follows;

$$Y(+2) = -\frac{X^{(2)}(+2)}{2}, \tag{5.54}$$

$$Y(+1) = -X^{(1)}(+1) - \frac{X^{(2)}(+1)}{2}, \tag{5.55}$$

$$Y(0) = -X^{(1)}(0) - \frac{X^{(2)}(0)}{2}, \tag{5.56}$$

$$Y(-1) = -X^{(1)}(-1) - \frac{X^{(2)}(-1)}{2}, \tag{5.57}$$

$$Y(-2) = -\frac{X^{(2)}(-2)}{2}. \tag{5.58}$$

It it obvious that this array contains the contribution of the hopping parameter expansion up to the next leading order.

In the same manner, we can get the contribution of the next next leading order of the hopping parameter expansion as follows;

$$X^{(3)}(+3) = \kappa Q_4^{(+)}(\mu_q = 0) X^{(2)}(+2), \tag{5.59}$$

$$X^{(3)}(+2) = \kappa Q_s X^{(2)}(+2) + \kappa Q_4^{(+)}(\mu_q = 0) X^{(2)}(1), \tag{5.60}$$

$$\begin{aligned} X^{(3)}(+1) =& \kappa Q_s X^{(2)}(+1) + \kappa Q_4^{(+)}(\mu_q = 0) X^{(2)}(0) \\ &+ \kappa Q_4^{(-)}(\mu_q = 0) X^{(2)}(+2), \end{aligned} \tag{5.61}$$

$$X^{(3)}(0) = \kappa Q_s X^{(3)}(0) + \kappa Q_4^{(-)}(\mu_q = 0) X^{(2)}(+1) + \kappa Q_4^{(+)}(\mu_q = 0) X^{(2)}(-1), \tag{5.62}$$

$$X^{(3)}(-1) = \kappa Q_s X^{(2)}(-1) + \kappa Q_4^{(+)}(\mu_q = 0) X^{(2)}(-2) + \kappa Q_4^{(-)}(\mu_q = 0) X^{(2)}(0), \tag{5.63}$$

$$X^{(3)}(-2) = \kappa Q_s X^{(2)}(-2) + \kappa Q_4^{(-)}(\mu_q = 0) X^{(2)}(-1), \tag{5.64}$$

$$X^{(3)}(-3) = \kappa Q_4^{(+)}(\mu_q = 0) X^{(2)}(-2). \tag{5.65}$$

The corresponding array $Y(n)$ in given as follows;

$$Y(+3) = -\frac{X^{(3)}(+3)}{3}, \tag{5.66}$$

$$Y(+2) = -\frac{X^{(2)}(+2)}{2} - \frac{X^{(3)}(+2)}{3}, \tag{5.67}$$

$$Y(+1) = -X^{(1)}(+1) - \frac{X^{(2)}(+1)}{2} - \frac{X^{(3)}(+1)}{3}, \tag{5.68}$$

$$Y(0) = -X^{(1)}(0) - \frac{X^{(2)}(0)}{2} - \frac{X^{(3)}(0)}{3}, \tag{5.69}$$

$$Y(-1) = -X^{(1)}(-1) - \frac{X^{(2)}(-1)}{2} - \frac{X^{(3)}(-1)}{3}, \tag{5.70}$$

$$Y(-2) = -\frac{X^{(2)}(-2)}{2} - \frac{X^{(3)}(-2)}{3}, \tag{5.71}$$

$$Y(+2) = -\frac{X^{(3)}(-3)}{3}. \tag{5.72}$$

Repeating this procedure up to N–th order of the hopping parameter expansion, we can finally obtain the following array $Y^{(1)}(n)$ for the noise vector $\eta^{(1)}$;

$$Y^{(1)}(\pm N) = -\frac{X^{(N)}(\pm N)}{N}, \tag{5.73}$$

$$Y^{(1)}(\pm(N-1)) = -\frac{X^{(N)}(\pm(N-1))}{N} - \frac{X^{(N-1)}(\pm(N-1))}{N-1}, \tag{5.74}$$

$$\vdots \tag{5.75}$$

$$Y^{(1)}(\pm 2) = -\sum_{i=2} \frac{X^{(i)}(\pm 2)}{i}, \tag{5.76}$$

$$Y^{(1)}(\pm 1) = -\sum_{i=1} \frac{X^{(i)}(\pm 1)}{i}, \tag{5.77}$$

$$Y^{(1)}(0) = -\sum_{i=1} \frac{X^{(i)}(0)}{i}. \tag{5.78}$$

Note that we need to calculate the array $Y^{(r)}(n)$ for each noise vector $\eta^{(r)}$.

Using a set of arrays $\{Y^{(r)}(n)\}$, we can obtain the logarithm of the fermion determinant at zero chemical potential for one configuration as follows;

$$\log\det D^{WF}(\mu_q = 0) = \sum_{i=-N}^{N} \left[\frac{1}{N_{noise}} \sum_{r=1}^{N_{noise}} \left(\eta^{(r)}\right)^\dagger Y^{(r)}(i) \right]. \tag{5.79}$$

At this stage, we need to recall the fact that the non–zero contribution of the trace in Eq.(5.40) comes only from closed loops on a lattice. Therefore, the non–zero contribution of Eq.(5.79) comes only from specific terms whose index i in Eq.(5.79) is multiples of N_t. Therefore, we can finally obtain the expression

$$\log\det D^{WF}(\mu_q = 0) = \sum_{j=-[N/N_t]}^{[N/N_t]} \left[\frac{1}{N_{noise}} \sum_{r=1}^{N_{noise}} \left(\eta^{(r)}\right)^\dagger Y^{(r)}(jN_t) \right]. \tag{5.80}$$

For finite quark chemical potential case, it it obvious that $\left(\eta^{(r)}\right)^\dagger Y^{(r)}(\pm jN_t)$ has the quark chemical potential dependence $e^{\pm j\mu_q/T}$. Consequently, the following formula can be obtained for any quark chemical potential case;

$$\log\det D^{WF}(\mu_q) = \sum_{j=-[N/N_t]}^{[N/N_t]} \left[\frac{1}{N_{noise}} \sum_{r=1}^{N_{noise}} \left(\eta^{(r)}\right)^\dagger Y^{(r)}(jN_t) \right] e^{j\mu_q/T}. \tag{5.81}$$

Figure5.1 shows some schematical examples of quark loops for the calculation of $Y(i)$. Here, we define the following coefficients W_n for later convenience.

$$W_n = \frac{1}{N_{noise}} \sum_{r=1}^{N_{noise}} \left(\eta^{(r)}\right)^\dagger Y^{(r)}(nN_t) \tag{5.82}$$

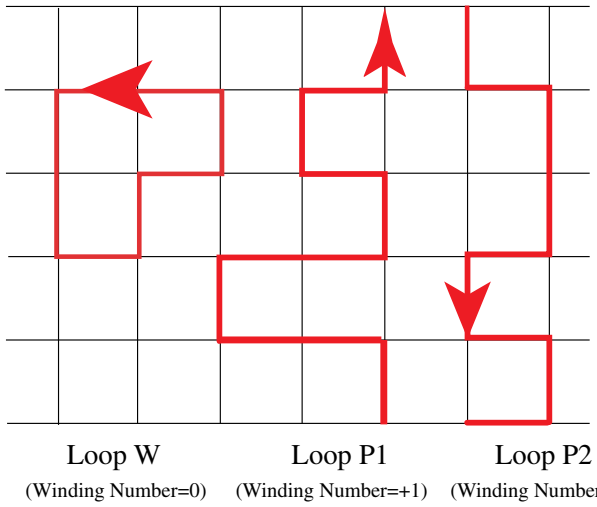

Figure 5.1: Schematical view for the calculation of $Y(i)$

Using a set of the coefficients $\{W_n\}$, we obtain the following expansion formula for the Wilson fermion determinant.

$$\det D^{WF}(\mu_q) = \exp\left[\sum_{n=-[N/N_t]}^{[N/N_t]} W_n \, e^{n\mu_q/T}\right] \tag{5.83}$$

Now, let us compare the numerical complexities for the reduction formula and the winding number expansion again. To come right to the point, time complexities for the reduction formula and the winding number expansion can be estimated to $O((N_xN_yN_z)^3 \times N_t)$ and $O(N_xN_yN_z \times N_t^3)$, respectively. Therefore, in an actual finite temperature-density system, numerical cost for the reduction formula is much higher than the winding number expansion in a large lattice. Moreover, as I stated before, the reduction formula needs much main memory because eigenvalues of a large–scale dense matrix must be calculated directly. To be more specific, we need main memory of approximately $(12N_xN_yN_z)^2 \times 16$ bytes at least in case of a double precision calculation in reduction formula. This procedure also hinders us from a numerical simulation on the large size of the lattice at this stage. However, in the winding number expansion, we do not need to deal with a large–scale dense matrix and there is no problem on main memory of a computer.

5.2.3 Summary of our numerical calculation for the winding number expansion method

In this section, we summarize essential features to construct the winding number expansion for reader's convenience.

1. The Wilson fermion matrix: $D^{WF}(\mu_q) = 1 - \kappa Q(\mu_q)$
2. The logarithm of the Wilson fermion matrix: $\log\det D^{WF} = \mathrm{Tr}\log(1 - \kappa Q) = -\sum_k \kappa^k \mathrm{Tr} Q^k/k$
3. All of Q_k makes quark hopping lines, but only closed lines remain in $\mathrm{Tr}Q^k$.
4. Wilson loops have no μ_q dependence (Loop W in Fig.5.1).
5. Only loops which wind along the temporal direction have μ_q dependence: $\exp(\pm k\mu_q a N_t) = \exp(\pm k\mu_q/T)$ (Loop P1 and P2 in Fig.5.1).
6. In calculation of $\mathrm{Tr}Q^k$, we use the noise method.
7. Finally, we construct $\det D^{WF}$ at any quark chemical potential $\mu_q \in \mathbb{C}$ with $\{W_n\}$ as follows;

$$\det D^{WF}(\mu_q) = \exp\left[\sum_{n=-[N/N_t]}^{[N/N_t]} W_n\, e^{n\mu_q/T}\right]. \tag{5.84}$$

Note that N is a number of maximum order of the hopping parameter expansion.

Chapter 6

Numerical results

In this chapter, my lattice design and my parameter setting are shortly introduced. Then, we discuss the validity of the noise method for numerical calculation of the trace that appears in the winding number expansion method. The multiple precision calculation for the Fourier transformation of the grand canonical partition function at purely imaginary chemical potential is also discussed. After that, the baryon chemical potential dependence of the thermodynamic observables (pressure, baryon number density, baryon susceptibility) are discussed.

6.1 Simulation parameters

In this work, we employ the Iwasaki gauge action in Eq.(2.53) and the two–flavor $O(a)$–improved Wilson fermion action in Eq.(2.47) with $C_{SW} = (1 - 0.8412/\beta)^{-3/4}$ evaluated by a one–loop perturbation theory [66]. All simulations to obtain thermodynamic quantities were performed with the following lattice volume;

$$N_x \times N_y \times N_z \times N_t = 8 \times 8 \times 8 \times 4. \tag{6.1}$$

Parameter sets for this work are summarized in table.6.1. The values of the hopping parameter κ were determined for each value of β by following the line of constant physics for the case of $m_\pi/m_\rho = 0.8$, as in Ref. [68].

We generated gauge configurations at zero baryon chemical potential using the hybrid Monte Carlo (HMC) method. The step size $d\tau$ and number of steps N_τ of HMC were set as $d\tau = 0.02$ and $N_\tau = 50$ so that the simulation

β	T/T_c	κ
2.00	1.35(7)	0.136931
1.95	1.20(6)	0.137716
1.90	1.08(5)	0.138817
1.85	0.99(5)	0.140070
1.80	0.93(5)	0.141139
1.70	0.84(4)	0.142871

Table 6.1: Parameters for numerical calculation.

time is $N_\tau d\tau = 1$. After the first 2000 trajectories to achieve the thermalization, we sampled a gauge configuration every 200 trajectories and collected 400 configuration for each parameter set.

6.2 Validity of the noise method for calculation of the trace

As explained in the previous section, we adopt a noise method to calculate the trace in Eq. (5.42). Therefore, the problem we have to verify is if fermion determinants obtained through the noise method are consistent with those calculated exactly by LU decomposition so that we can safely neglect errors from the truncation in the noise method. To check this, we calculate fermion determinants at various values of purely imaginary chemical potential using both the noise method and LU decomposition at $T/T_c = 1.08$ as a test. In this test analysis, we adopt the Iwasaki gauge action and the standard Wilson fermion action on a 4^4 lattice, and fermion determinants are averaged over 100 configurations generated at zero quark chemical potential. We use 16 noise vectors for the traces appearing in the winding number expansion. Figure 6.1 shows that the noise method can produce consistent results with those obtained by LU decomposition within the range of statistical errors. It should be noted that the error bars in Fig.6.1 are attributed to fluctuations over 100 configurations, and exactly the same magnitude of the error bars must be reproduced if the noise method works properly. Consequently, our winding number expansion method with the noise vectors works reliably in our analyses and we do not have to take account of errors from this part of the approximation.

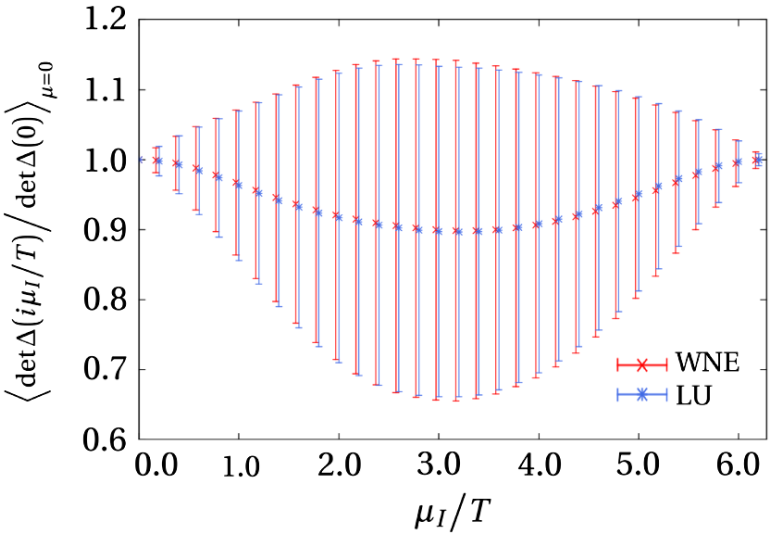

Figure 6.1: Pure imaginary chemical potential dependence of fermion determinants. Red and blue points are calculated by the winding number expansion with 16 noise vectors and LU decomposition, respectively. Error bars reflect the statistical error and they are estimated by Jackknife method.

6.3 Validity of multiple precision calculation

We actually monitored the behavior of all variables in the DFT process to study the effects of the cancellation of significant digits and the loss of trailing digits. As a result, we found that the cancellation of significant digits is not negligible in the DFT program and Fig.6.2 shows canceled digits in our DFT program. We also found that the cancellation of significant digits occurs regardless of temperatures in our system. To overcome this problem, we adopt multiple precision calculation for DFT as stated in the previous chapter. Figure 6.3 shows the effect of canceled digits in the calculation of Z_B with $16, 32, 48$, and 64 significant digits. According to this figure, when evaluating Z_B for a large baryon number B, it is essential to increase the number of significant digits of the variables in the DFT. In this work, we calculate the Fourier transformation with 400 significant digits.

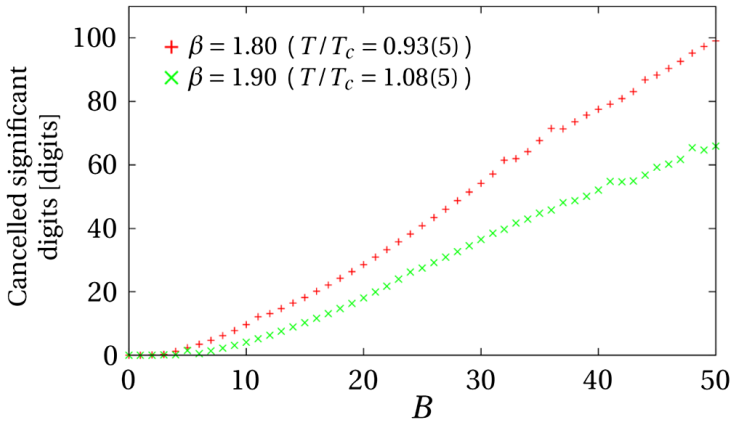

Figure 6.2: Canceled significant digits in the DFT calculation at temperatures above (upper red points) and below (lower green points) T_c

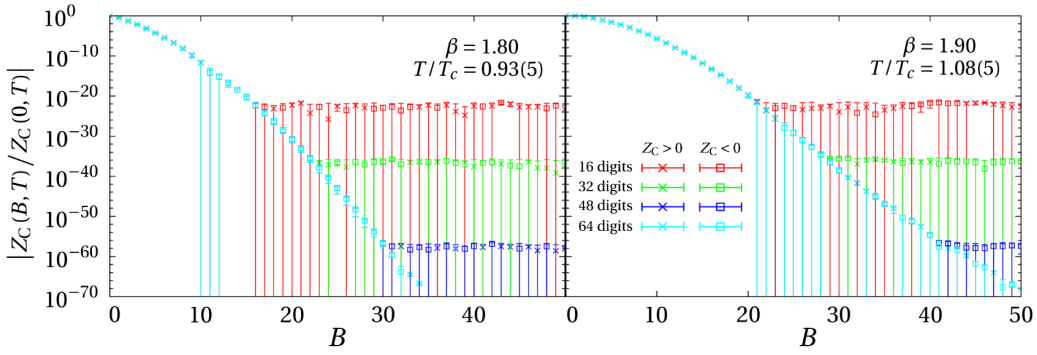

Figure 6.3: Relationship between the behavior of Z_B and the precision of the variables in the DFT at temperatures above (right) and below (left) T_c. Both include 16 (double precision, upper red points), 32 (second green points), 48 (third blue points), and 64 (lowest cyan points) significant figures. Errors are estimated by Jackknife method.

6.4 Calculation process in lattice simulation

Coefficients of the winding number expansion $\{W_n\}$ in Eq.(5.84) were computed up to $n = 120$ using the hopping parameter expansion up to the 480–th order with 400 configurations in all temperature cases. We used 64 and 128 noise vectors for temperatures above and below T_c, respectively, to calculate the trace in the fermion determinant. In section 6.3, we confirmed that 16 noise vectors can reproduce the consistent results with exact ones for a 4^4 lattice case. Thus, from simple extrapolation to make the number of the noise vectors proportional to the lattice size, we anticipate that we need to use 128 noise vectors to ensure the same precision for a $8^3 \times 4$ case. Imposing the relation $W_n = W^*_{-n}$ on the numerical results reduces the necessary number of the noise vectors by a half. Therefore, we conclude that 64 noise vectors for a $8^3 \times 4$ lattice are sufficient to achieve the same precision with 16 noise vectors for a 4^4 lattice. We note that the previous work[67] used only 16 noise vectors for a $8^3 \times 4$ lattice case. In addition, we checked that thermodynamic observables with $\{W_n\}$ up to $n = 120$ are identical, apart from negligibly small deviation, with those with $\{W_n\}$ up to $n = 110$ with the direct method explained in section 6.6.

We evaluated the grand canonical partition functions at various pure imaginary chemical potentials using the winding number expansion with the sets of $\{W_n\}$. After that, we evaluated the normalized canonical partition function $Z_B/Z_{B=0}$ through the Fourier transformation and the thermodynamic observables. In the following, Z_B denotes the normalized canonical partition function for notational brevity. For our calculations other than the generation of gauge configurations and the calculation of W_n, the multiple precision calculation was adopted with 400 significant digits to ensure sufficient precision. The gauge configurations and the sets of W_n were computed with double precision, i.e., 16 significant digits.

6.5 Numerical results of the canonical partition function $Z_B(T)$

Figure 6.4 shows the behavior of canonical partition functions at all temperatures. Because these results satisfy the relation

$$Z_B(T) = Z_{-B}(T), \tag{6.2}$$

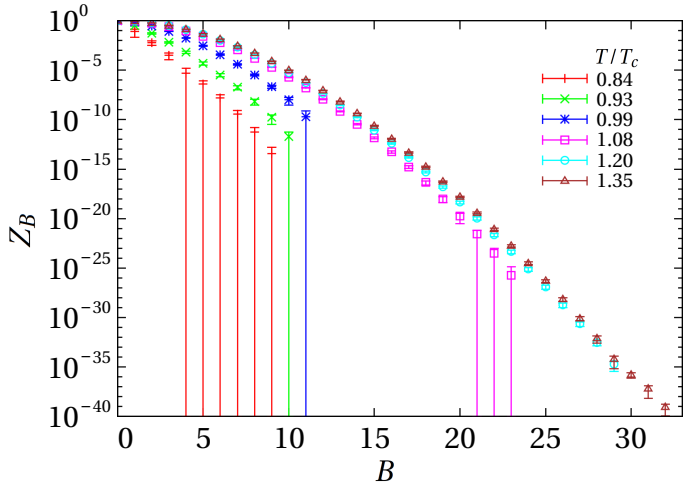

Figure 6.4: Temperature dependence of canonical partition functions. The vertical axis is in log scale. The red, green, blue, magenta, light blue, and brown points are the results at $T/T_c = 0.84, 0.93, 0.99, 1.08, 1.20$, and 1.35 respectively. Error bars reflect the statistical error and they are estimated by Jackknife analysis.

which originates from the symmetry between a particle and an anti–particle, the region for $B \geq 0$ only is plotted for convenience. From this figure, it can be said that the canonical partition function rapidly decreases as a baryon number B becomes large. This behavior is quite natural considering the fugacity expansion of the grand canonical partition function. In the grand canonical ensemble, $Z_B(T)e^{B\mu_B/T}/Z_{GC}(T,\mu_B)$ corresponds to the probability for the realization of the states whose baryon number is B at (T,μ_B). Therefore, the behavior of the canonical partition functions can be understood from the fact that the states whose baryon number is large is less likely to be realized. Figure 6.4 also tells us that the lower the temperature becomes, the more rapidly the canonical partition functions decrease. This behavior originates from the thermal weight. The statistical error becomes larger as the temperature becomes lower especially below T_c. One of the reasons for this error behavior is that we need to deal with smaller values in the Fourier transformation for lower temperatures.

6.6 Results of thermodynamic observables

In this section, we analyze the chemical potential dependence of the thermodynamic observables calculated by the direct method and the canonical approach. In the direct method, the winding number expansion

$$\det D^{WF}(\mu_B) = \exp\left[\sum_{n=-\infty}^{\infty} W_n e^{n\mu_B/T}\right] \tag{6.3}$$

is used for the calculation of the thermodynamic observables at a real baryon chemical potential. When we calculate the thermodynamic observables, the imaginary part of the thermodynamic observables is not zero for each configuration. The imaginary part should be consistent with zero within the statistical error after taking the statistical average over gauge configurations. Therefore, in this work, the behavior of the imaginary part of the thermodynamic observable is used to judge the validity ranges of the baryon chemical potential in the direct method and the canonical approach. In the following, we consider the thermodynamic observables at $T/T_c = 1.08$ as examples to explain the strategy. Comparing the thermodynamic observables computed by the direct method and the canonical approach, we check the consistency between these methods. In addition, we also compare our canonical results with those obtained by the multi–parameter reweighing (MPR) method with the same numerical setup as Ref.[59]. It is known that the MPR method is valid and frequently used for a low density system. In Ref.[59], the authors also discussed the consistency between the MPR and the Taylor expansion methods and concluded that both methods produced consistent results in the small chemical potential region where statistical errors of both methods could be under control. Therefore, our present work enables us to augment the consistency check among our canonical approach, the MPR method, and the Taylor expansion method.

6.6.1 Estimation of validity range of the direct method and the canonical approach

Figures 6.5, 6.6, and 6.7 show the imaginary part of the pressure, the baryon number density, and baryon susceptibility, respectively, obtained by the direct method and the canonical approach at $T/T_c = 1.08$. These figures tell us that the imaginary part of the thermodynamic observables calculated by

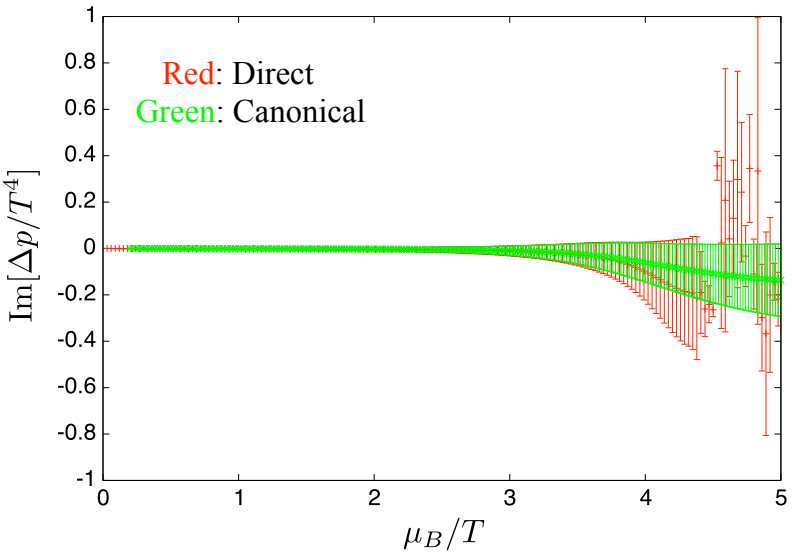

Figure 6.5: Baryon chemical potential dependence of the imaginary part of the pressure. The red and green points are the results calculated by the direct method and the canonical approach at $T/T_c = 1.08$. Error bars reflect the statistical error and they are estimated by Jackknife analysis.

the direct method and the canonical approach is consistent with zero within the statistical errors over the baryon chemical potential region shown the figure. To estimate the validity range of the baryon chemical potential quantitatively in the direct method and the canonical approach, we focus on how large the statistical errors are. From Fig.6.8, it is found that the statistical errors of the imaginary part of the pressure are always smaller in the canonical approach than in the direct method up to around $\mu_B/T \sim 4.4$. In the canonical approach, we first determine the maximum value of the baryon chemical potential μ_B^{max} in a way that we will explain soon later. We estimate the magnitude σ_1 of the statistical error of the imaginary part of the thermodynamic observables at μ_B^{max1}/T. Then, in the direct method, we determine the maximum value of the baryon chemical potential μ_B^{max2}/T from the condition that the magnitude of the statistical error coincides with σ_1. Now let us explain how to determine μ_B^{max1}/T below.

In our numerical calculations, the fugacity expansion of the grand canon-

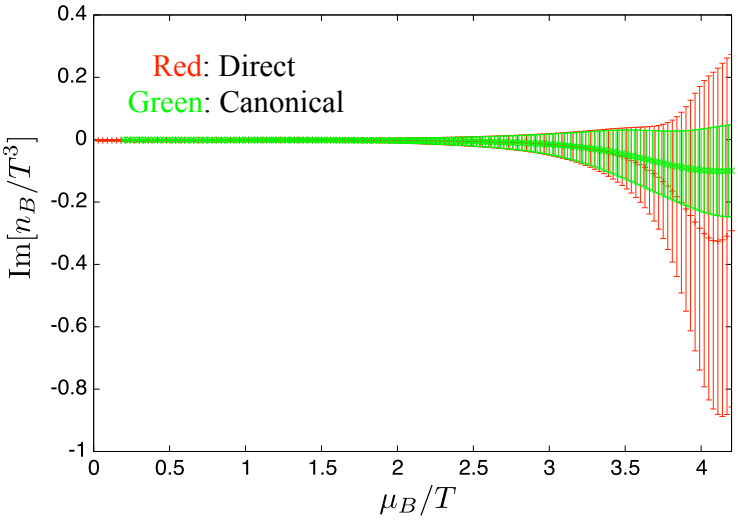

Figure 6.6: Baryon chemical potential dependence of the imaginary part of the baryon number density. The red and green points are the results calculated by the direct method and the canonical approach at $T/T_c = 1.08$. Error bars reflect the statistical error and they are estimated by Jackknife analysis.

ical partition function must be truncated with finite series as

$$Z_{GC}(T, \mu_B) = \sum_{B=-N_{max}}^{N_{max}} Z_B(T) e^{B\mu_B/T}. \tag{6.4}$$

The method to analyze the effect of the truncation error is as follows. First, we evaluate expectation values $\langle O(\mu_B)\rangle_{N_{\rm max}}$ using Eq.(6.4). Next, we calculate expectation values $\langle O(\mu_B)\rangle_{N_{\rm max}-1}$ in Eq.(6.4). We then evaluate the relative error $R_{\rm ob}(\mu_B)$ from these expectation values as

$$R_{\rm ob}(\mu_B) \equiv 1 - \frac{\langle O(\mu_B)\rangle_{N_{\rm max}-1}}{\langle O(\mu_B)\rangle_{N_{\rm max}}}. \tag{6.5}$$

In this study, we choose $R_{\rm ob}(\mu_B) < 10^{-3}$ as a reliability criterion.

Using this criterion, we can deduce that the validity range of the baryon chemical potential for the pressure is $\mu_B/T \lesssim 5$. From this value of the baryon chemical potential and the method as explained above, we can conclude that the validity range is $\mu_B/T \lesssim 3.7$ in the direct method. In this

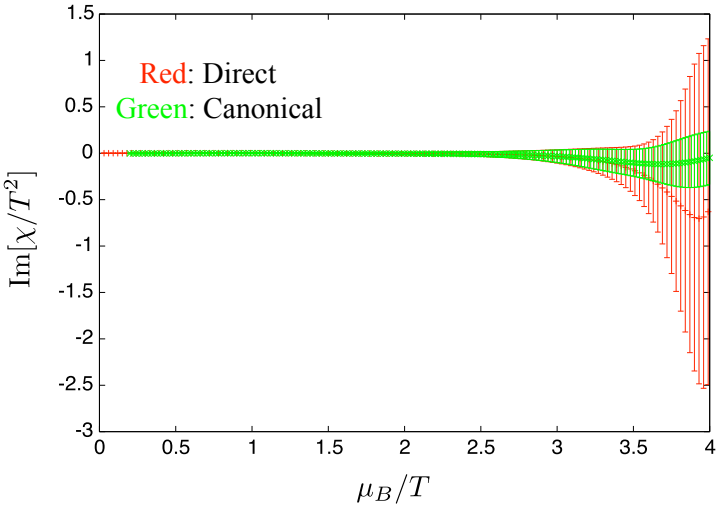

Figure 6.7: Baryon chemical potential dependence of the imaginary part of the baryon susceptibility calculated. The red and green points are the results calculated by the direct method and the canonical approach at $T/T_c = 1.08$. Error bars reflect the statistical error and they are estimated by Jackknife analysis.

work, the validity ranges of the baryon chemical potential for all other thermodynamic observables are determined likewise.

6.6.2 Baryon chemical potential dependence of pressure

First, we examine the pressure. Figure 6.9 shows the baryon chemical potential dependence of the pressure calculated by the canonical approach and the direct method at $T/T_c = 1.35, 1.20, 1.08, 0.99, 0.93$, and 0.83. From this figure, we see that the pressure calculated by the canonical approach above T_c do not suffer from large errors up to $\mu_B/T \simeq 5$, and the results below T_c are reliable up to $\mu_B/T \simeq 3$. In contrast, the results computed by the canonical approach just below T_c are reliable only up $\mu_B/T \simeq 3$. This is possibly because we generated gauge configurations at zero quark chemical potential, and they have enhanced fluctuations caused by the phase transition. We may have obtained clearer signals if we generated gauge configurations at pure imaginary chemical potentials because T_c at a pure imaginary chem-

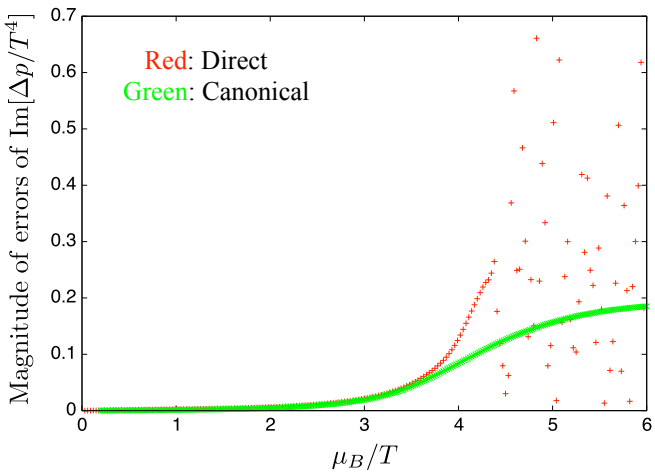

Figure 6.8: Baryon chemical potential dependence of the magnitude of the statistical errors of the imaginary part of the pressure at $T/T_c = 1.08$.

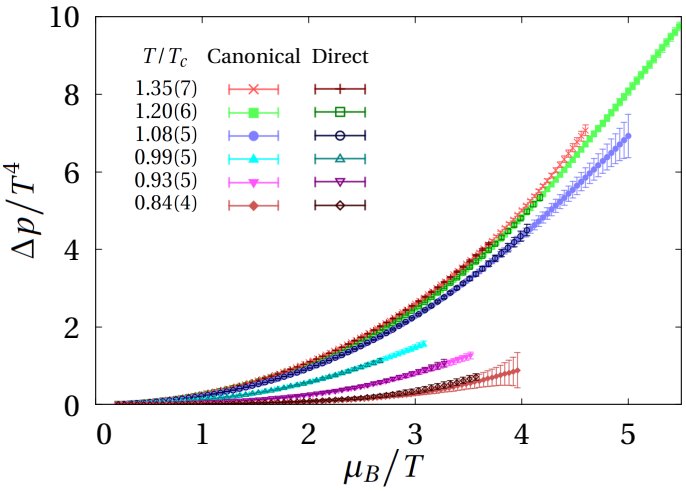

Figure 6.9: Baryon chemical potential dependence of the pressure calculated by the canonical approach and the direct method at $T/T_c = 1.35, 1.20, 1.08, 0.99, 0.93,$ and 0.83. Error bars reflect the statistical error and they are estimated by Jackknife analysis.

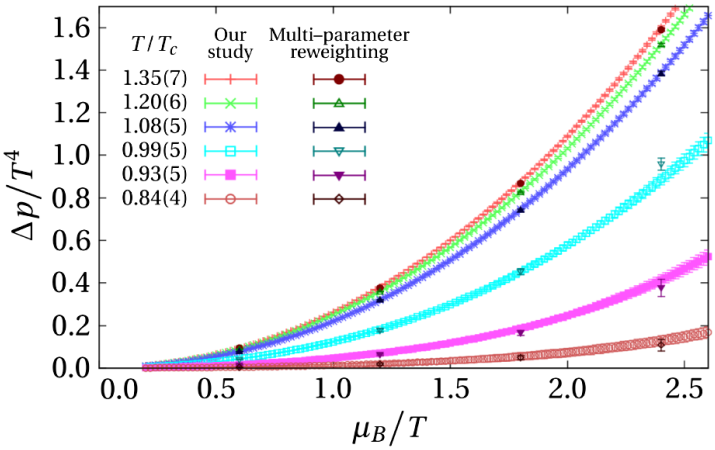

Figure 6.10: Comparison of the pressure calculated by the canonical approach and the MPR method. The colors of the data points are the same as in Fig.6.9 with some additional colors. The data points plotted in the additional colors of dark red, dark green, dark blue, dark cyan, dark magenta, and dark brown points are the results at $T/T_c = 1.35, 1.20, 1.08, 0.99, 0.93$, and 0.83, respectively, as calculated by the MPR method.

ical potential is higher than that at zero chemical potential. In addition, Fig.6.9 tells us that the results calculated by the canonical approach agree very well with those calculated by the direct method within the statistical error. This is an evidence supporting that the canonical approach does not lose any physical information that the direct way should have. Figure 6.10 shows that the pressure calculated by the canonical approach also agrees very well with the pressure obtained using the MPR method. Moreover, this figure tells us that our canonical approach can provide us with the results at larger baryon chemical potential.

6.6.3 Baryon chemical potential dependence of baryon number density

In this subsection, we consider the expectation value of the baryon number density. Figure 6.11 demonstrates that for temperatures above T_c (and blow T_c), the results calculated by the canonical approach are reliable up to $\mu_B/T \simeq 4$ (and $\mu_B/T \simeq 3 \sim 3.5$, respectively). The reliable baryon chemical

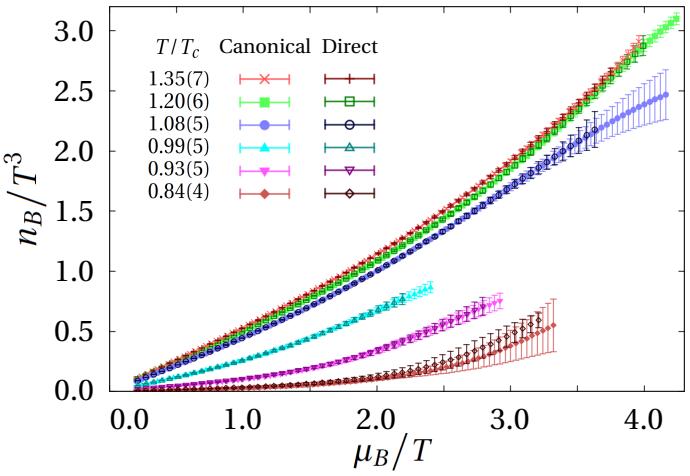

Figure 6.11: Baryon chemical potential dependence of the baryon number density calculated by he canonical approach and the direct method at $T/T_c = 1.35, 1.20, 1.08, 0.99, 0.93$, and 0.83. Error bars reflect the statistical error and they are estimated by Jackknife analysis.

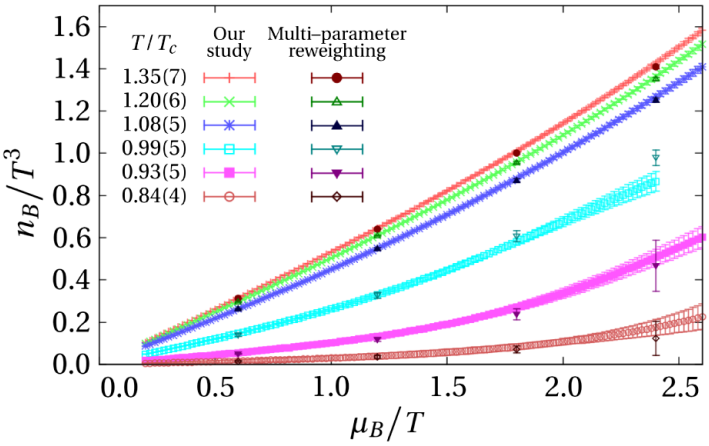

Figure 6.12: Comparison of baryon number density calculated by the canonical approach and the MPR method. The colors of the data points are the same as in Fig.6.10

potential range for temperatures just below T_c is limited $\mu_B/T \lesssim 2.4$. This is possibly because of the same reason as in the pressure case. In addition, Fig.6.11 tells us that the results calculated by the canonical approach agree very well with those calculated by the direct method within the statistical errors. Figure 6.12 demonstrates good agreement between the results of the canonical approach and the MPR method. Moreover, we see that the slope of n_B/T^3 becomes smaller as the temperature decreases. In zero temperature case, n_B should be zero up to $\mu_B/T = m_B/T$, where m_B is the lightest baryon mass in the system, and thus the slope is completely flat then. The data at $T/T_c = 0.84$ in Fig.6.11 does in fact show such a tendency. In case of the analyses of the baryon number density, it can be said again that our canonical approach can provide us with the results at larger baryon chemical potential.

6.6.4 Baryon chemical potential dependence of baryon number susceptibility

Finally, we investigate the baryon number susceptibility. Figure 6.13 shows that the results obtained by the canonical approach at temperatures above T_c are reliable up to $\mu_B/T \simeq 3.5.$, whereas those at temperatures below T_c are reliable up to $\mu_B/T \simeq 2.4 \sim 2.9$. In addition, Fig.6.13 tells us that the results calculated by the canonical approach agree very well with those calculated by the direct method within the statistical errors. From Fig.6.14, we find that the susceptibility results in the canonical approach are in very good agreement with those of the MPR method. Moreover, Fig.6.14 tells us that our canonical method produces fewer statistical errors than the MPR and the Taylor expansion method even at small baryon chemical potential for the same number of gauge configurations.

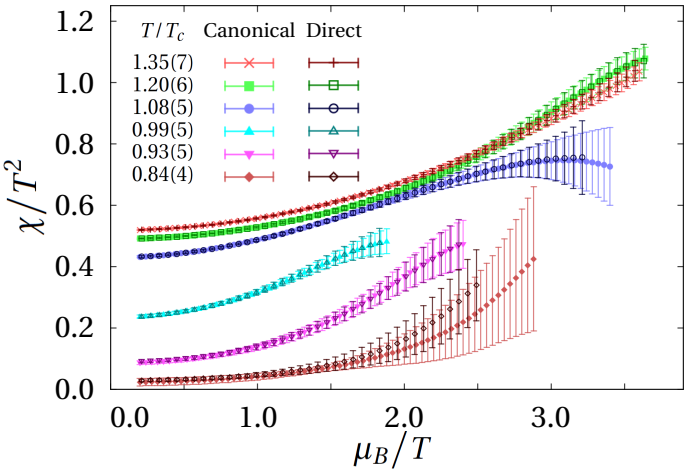

Figure 6.13: Baryon chemical potential dependence of the baryon number susceptibility calculated by both the canonical approach and the direct method explained in previous section at $T/T_c = 1.35, 1.20, 1.08, 0.99, 0.93,$ and 0.83. Error bars reflect the statistical error and they are estimated by Jackknife analysis.

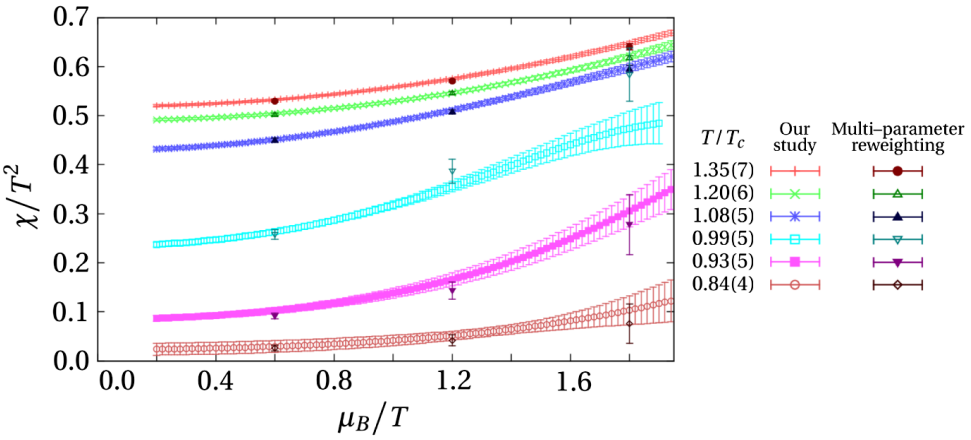

Figure 6.14: Comparison of the baryon number susceptibility calculated by the canonical approach and the MPR method. The colors of the data points are the same as in Fig.6.10

Chapter 7

Summary and outlook

In this thesis, the canonical approach as a method for finite density QCD is studied in detail. Because the fermion determinant becomes complex in finite density QCD in general, the Monte Carlo integration with the complex fermion determinant does not work. This is the sign problem. In the case of the canonical approach, the fermion determinant is kept to be real and the Monte Carlo method can work safely.

The grand canonical partition function $Z_{GC}(\mu_q, T)$ is expressed as the fugacity expansion with the expansion coefficients given by the canonical partition functions $Z_n(T)$. The canonical partition functions $\{Z_n\}$ can be obtained by the Fourier transformation of the grand canonical partition function calculated at purely imaginary chemical potential. In the theory with purely imaginary chemical potential, the fermion determinant is real and the grand canonical partition function can be evaluated using a standard Monte Carlo method for lattice QCD simulation. Therefore, we can calculate the canonical partition functions without the sign problem. This means that, once $\{Z_n\}$ are given, we can compute the grand canonical partition function for any real chemical potential via the fugacity expansion. However, we encounter some difficulties inherent in the canonical approach as a price to pay for avoiding the sign problem. In the calculation to obtain the canonical partition function at large baryon number, the Fourier transformation becomes a highly oscillating integral. Thus, it is difficult to numerically compute the integral because of cancellation of significant digits in the Fourier transformation. To avoid this problem, the multiple precision computation was adopted and the validity was also checked in this work. Another problem is the numerical cost for the calculation of fermion determinants. To perform

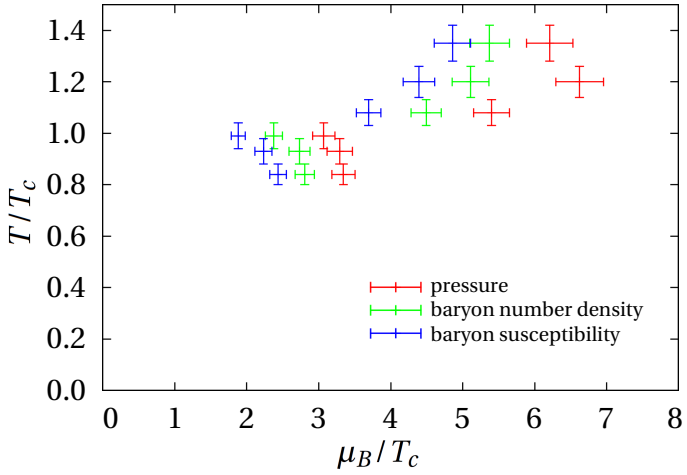

Figure 7.1: Upper bound of the baryon chemical potential μ_B/T_c in the calculation of thermodynamic observables using the canonical approach. Error bars reflect the error originated from the determination of the pseudo critical temperature T_c at vanishing baryon chemical potential.

the Fourier transformation, the grand canonical partition functions at many different values of purely imaginary chemical potential are needed. An ideal way to calculate the fermion determinant is to adopt the reduction formula that is exact. However, the numerical cost for the reduction formula increases as $O((N_x N_y N_z)^3 \times N_t)$. Moreover, the reduction formula needs much more memory. Even considering recent computer resources, we cannot perform numerical simulation with a large lattice size using the reduction formula. To reduce this numerical cost, the winding number expansion method of the fermion determinant is developed in this work. The numerical cost for the winding number expansion increases as $O(N_x N_y N_z \times N_t^3)$ and we do not need to store any matrices in this case and so we can save the memory.

Using the above method, our canonical approach could provide reliable results beyond $\mu_B/T \simeq 3$ for all thermodynamic observables (except for the case near T_c). Figure 7.1 summarizes the upper bounds of the baryon chemical potential μ_B normalized by the critical temperature T_c using the canonical approach. From this figure, it is found that the validity range of the calculation for the pressure is wider than that for the baryon number density and the baryon number susceptibility. This is because derivatives in terms of μ_B/T are included in the baryon number density and the number

baryon susceptibility, which makes the convergence of the fugacity expansion worse.

In addition, we also compared our results obtained by the canonical approach with those obtained by the direct calculation with the winding number expansion. In this analysis, we could check that these results are consistent and no physical information is lost in the canonical approach. This is very encouraging for future developments on finite density QCD based on the first–principles calculation. We note that the validity range is so far limited up to $\mu_B/T \simeq 3$ in other methods such as the multi-parameter reweighting method, the Taylor expansion, the imaginary chemical potential, and the density of states method. Thus, it can be said that the canonical approach could be one of the most promising candidates to overcome the sign problem.

Getting more reliable signals in a large baryon chemical potential region with the canonical approach, we need to calculate the canonical partition functions more accurately at large baryon numbers. In this work, we calculate the grand canonical partition functions at all pure imaginary chemical potential with the gauge configurations generated at zero chemical potential through the simplest reweighting method. However, we could have calculated them with gauge configurations generated at suitable pure imaginary chemical potentials to realize the appropriate importance sampling as follows;

$$Z_{GC}(i\mu_I) = \frac{1}{N}\sum_{i=1}^{N}\int [dU]\left[\frac{\det\Delta(i\mu_I)}{\det\Delta(i\mu_i)}\right]\det\Delta(\mu_i)\, e^{-S_g} \quad (\mu_i \in \mathbb{R}). \tag{7.1}$$

This is one of the future problems to be studied.

The canonical approach has been investigated in the several previous studies [69, 70, 71, 72, 73]. Our method may be improved further to obtain results under more realistic conditions, i.e., lighter quark mass, larger volume, finer lattice spacing, and higher density. In particular, the following strategy could give us successful results to achieve simulations with lighter quarks for example. Let us consider the identity transformation of the logarithm of the fermion determinant for Wilson fermions;

$$\begin{aligned}\log\det D^{WF}(\mu_q) &= \mathrm{Tr}\log\Big(1-\kappa Q_s-\kappa Q_t(\mu_q)\Big)\\ &= \mathrm{Tr}\log(1-\kappa Q_s)+\mathrm{Tr}\log\left(1-\kappa\frac{1}{1-\kappa Q_s}Q_t(\mu_q)\right).\end{aligned} \tag{7.2}$$

Here, Q_s and Q_t in Eq.(7.2) represent propagations of the fermions in three dimensional space and along the time direction, respectively. In an ac-

tual numerical calculation, we do not need to consider the contribution from the first term in Eq.(7.2). This is because we have only to evaluate $\left\langle \det D^{WF}(i\mu_I)/\det D^{WF} \right\rangle$ to obtain the grand canonical partition functions at purely imaginary chemical potential and the first term in Eq.(7.2) has no contribution to this quantity. Using this identity transformation, we expand the second term in Eq.(7.2) in terms of κ and the following approximation formula can be obtained;

$$\mathrm{Tr}\log\left(1-\kappa\frac{1}{1-\kappa Q_s}Q_t(\mu_q)\right) = -\sum_{n=1}^{\infty}\frac{\kappa^n}{n}\mathrm{Tr}\left[\frac{1}{1-\kappa Q_s}Q_t(\mu_q)\right]^n. \qquad (7.3)$$

Note that the factor $D_s^{-1} = 1/(1-\kappa Q_s)$ physically corresponds to a quark propagator in three dimensional space. Therefore, this expansion can evaluate the exact quark propagations in three dimensional space and the hopping parameter expansion is used to estimate the contribution of quark propagations only in the time direction. In this improved expansion, D_s^{-1} needs to be calculated in advance and operated to a vector X with color, Dirac, and spacetime indices many times in an actual simulation. The number of elements of the factor D_s^{-1} is $(12N_{\mathrm{V}})^2$, where N_{V} is $N_x \times N_y \times N_z$ and the factor 12 comes from the degree of freedoms of color and Dirac space. Therefore, numerical costs to obtain D_s^{-1} and to operate the factor to the vector X are more expensive than the winding number expansion because D_s^{-1} is a dense large–scale matrix in general. An idea to overcome this difficulty is to solve an equation $X = D_s \times Y$ in terms of Y by the conjugate gradient method instead of calculating $Y = D_s^{-1} \times X$. Using the conjugate gradient method, the approximate solution $\tilde{Y}$ can be evaluated iteratively with the stopping condition $|X - D_s\tilde{Y}|^2 < \epsilon$ and the exact solution Y can be obtained by $12N_{\mathrm{V}}$ times iterations. Because D_s is a sparse matrix, we could hope that the number of the iterations are much less than $12N_{\mathrm{V}}$ even if we adopt a suitable stopping condition. The fact that we do not need to calculate D_s^{-1} in advance is also a strong point of this strategy with conjugate gradient method.

Although the hopping parameter expansion yielded very interesting results in this study, the final step is to calculate the fermion determinant without this approximation; we have learned from this study that the key point is to calculate the determinant at imaginary chemical potential values that can undergo the Fourier transformation with high accuracy. This requires more computational resources than what has been reported here but

is within the scope of the next-generation high-performance computing.

Acknowledgement

First of all, I would like to thank my teachers, my family and my friends, and all the people for supporting me to write this Ph.D thesis. Especially, I would like to thank my supervisor Kenji Fukushima for all his help in my studies, his continuous encouragement, and his hospitality. I am also very grateful to Atsushi Nakamura and Shotaro Oka for the collaboration on the topics included in this Ph.D thesis.

Bibliography

[1] C. Patrignani *et al.* (Particle Data Group), Chin. Phys. C, **40**, 100001 (2016)

[2] H. D. Politzer, Phys. Rev. Lett. 30, (1973) 1346

[3] D. J. Gross and F. Wilczek, Phys. Rev. Lett. 30, (1973) 1343

[4] K. Fukushima and T. Hatsuda, Rept. Prog. Phys. **74**, 014001 (2011)

[5] M. Fukugita, M. Okawa, and A. Ukawa, Nucl. Phys. B **337** (1990) 181

[6] Y. Aoki, G. Endrodi, Z. Fodor, S. D. Katz, and K. K. Szabo, Nature **443** (2006) 675–678

[7] C. DeTar, U. M. Heller, Eur. Phys. J. A **41** (2009) 405–437

[8] T. Bhattacharya *et al.*, Phys. Rev. Lett. 113, (2014) 082001

[9] M. Asakawa, K. Yazaki, Nucl. Phys. A **504** (1989) 668–684

[10] A. Barducci, R. Casalbuoni, S. De Curtis, R. Gatto, and G. Pettini, Phys. Lett. B **231** (1989) 463

[11] F. Wilczek, Int. J. Mod. Phys. **A7** (1992) 3911–3925

[12] J. Berges, K. Rajagopal, Nucl. Phys. B **538** (1999) 215–232

[13] M. A. Stephanov, PoS LAT 2006, (2006) 024

[14] A. Barducci, R. Casalbuoni, S. De Curtis, R. Gatto, and G. Pettini, Phys. Rev. D **41** (1990) 1610

[15] A. Barducci, R. Casalbuoni, G. Pettini, and R. Gatto, Phys. Rev. D **49** (1994) 426

[16] M. A. Halasz, A. D. Jackson, R. E. Shrock, M. A. Stephanov, and J. J. M. Verbaarschot, Phys. Rev. D **58** (1998) 096007

[17] O. Scavenius, A. Mocsy, I. N. Mishustin, and D. H. Rischke, Phys, Rev. C **64** (2001) 045202

[18] N. G. Antoniou and A. S. Kapoyannis, Phys. Lett. B **563** (2003) 165

[19] Y. Hatta and T. Ikeda, Phys. Rev. D **67** (2003) 014028

[20] A. Barducci, R. Casalbuoni, G. Pettini, and L. Ravagli, Phys. Rev. D **72** (2005) 056002

[21] S. Roessner, C. Ratti, and W. Weise, Phys. Rev. D **75** (2007) 034007

[22] Z. Fodor, S. D. Katz, JHEP **0203** 014 (2002) [arXiv:0106002[hep-lat]]

[23] Z. Fodor, S. D. Katz, JHEP **0404** 050 (2004) [arXiv:0402006[hep-lat]]

[24] S. Ejiri, C. R. Allton, S. J. Hands, O. Kaczmarek, F. Karsch, E. Laermann, and Ch. Schmidt, Prog. Theor. Phys. Suppl. **153**, 118 (2004)

[25] M. G. Gavai, S. Gupta, Phys. Rev. D **71**, 114014 (2005)

[26] T. Kunihiro, Phys. Lett. B **271**, 395 (1991)

[27] T. Hatsuda and T. Kunihiro, Phys. Rept. **247**, 221 (1994)

[28] M. Asakawa, S. Ejiri, and M. Kitazawa, Phys. Rev. Lett. **103** 262301 (2009)

[29] M. A. Stephanov, Phys. Rev. Lett. **102** 032301 (2009)

[30] M. M. Aggarwal *et al.* (STAR Collaboration), Phys. Rev. Lett. **105** 022302 (2010)

[31] X. Luo, J. Phys. G **39** 025008 (2012)

[32] X. Luo, Phys. Rev. C **91** 034907 (2015)

[33] UKQCD collaboration, I. M. Barbour, Nucl. Phys. **A642** (1998) 251–262

[34] C. R. Allton, S. Ejiri, S. J. Hands, O. Kaczmarek, F. Karsch, E. Laermann, Ch. Schmidt, L. Scorzato (Bielefeld-Swansea), Phys. Rev. D **66**, 074507 (2002). [arXiv:0204010[hep-lat]]

[35] C. R. Allton, M. Doering, S. Ejiri, S. J. Hands, O. Kaczmarek, F. Karsch, E. Laermann, K. Redlich, Phys. Rev. D **71**, 054508 (2005). [arXiv:0501030[hep-lat]]

[36] M. G. Gavai, S. Gupta, Phys. Rev. D **78**, 114503 (2008). [arXiv:0806.2233[hep-lat]]

[37] M. G. Alford, A. Kapustin, F. Wilczek, Phys. Rev. D **59**, 054502 (1999). [arXiv:9807039[hep-lat]]

[38] Ph. de Forcrand, O. Philipsen, Nucl. Phys. B642 (2002), 290. [arXiv:0205016 [hep-lat]]

[39] A. Gocksch, Phys. Rev. Lett. **61** 2054 (1988).

[40] S. Ejiri, Phys. Rev. D **77** 014508 (2008). [arXiv:0706.3549[hep-lat]]

[41] Z. Fodor, S. D. Katz, C. Schmidt, JHEP **03** 121 (2007). [arXiv:0701022[hep-lat]]

[42] Ph. de Forcrand PoS (LAT2009)010, 2009.

[43] A. Nakamura, Phys. Lett. 149B (1984) 391.

[44] A. Hasenfratz and D. Toussaint, Nucl. Phys B371 (1992), 539.

[45] A. Nakamura, S. Oka and Y. Taniguchi, arXiv:1504.04096 [hep-lat].

[46] A. Nakamura, S. Oka and Y. Taniguchi, arXiv:1504.04471.

[47] I. M. Barbour and Z. A. Sabeur, Nucl. Phys, B 342, 269 (1990).

[48] X. -F. Meng, A. Li, A. Alexandru and K. -F. Liu, PoS LATTICE **2008**, 032 (2008) [arXiv:0811.2112 [hep-lat]].

[49] C. Gattringer and H. -P. Schadler, Phys. Rev. D 91, 074511 (2015) [arXiv:1411.5133].

[50] A. Nakamura and K. Nagata, Prog. Theor. Exp. Phys. (2016) 033D01 [arXiv:1305.0760]

[51] C. N. Yang and T. D. Lee, Phys. Rev. **87**, 404 (1952), T. D. Lee and C. N. Yang, Phys. Rev. **87** (1952) 410.

[52] R. Fukuda, A. Nakamura, and S. Oka, Phys. Rev. D **93**, 094508 (2016)

[53] R. Fukuda, A. Nakamura, and S. Oka, Proceeding of Science (LATTICE 2015) 167 (2015)

[54] K. G. Wilson, Phys. Rev. D **10**, 2445 (1974)

[55] K. G. Wilson, *Quarks and strings on a Lattice*, in "Gauge Theories and Modern Field Theory", MIT Press, Cambridge, 1975.

[56] K. G. Wilson, *Quarks and strings on a Lattice*, in "New Phenomena in Subnuclear Physics", Plenum Press, New York, 1977.

[57] P. Hasenfratz and F. Karsch, Phys. Lett. B **125**, 308 (1983)

[58] S. Muroya, A. Nakamura, C. Nonaka, T. Takaishi, Prog. Theor. Phys. 110, (2003) 615

[59] K. Nagata and A. Nakamura JHEP, 1204, 092 (2012). [arXiv:1201.2765].

[60] A. Roberge and N. Weiss, Nucl. Phys. B275(1986) 734.

[61] P. de Forcrand and S. Kratochvila, Nucl. Phys. Proc. Suppl. **153**, 62 (2006) [hep-lat/0602024].

[62] J. Danzer and C. Gattringer, Phys. Rev. D 78, 114506 (2008). [arXiv:08092736].

[63] K. Nagata and A. Nakamura, Phys. Rev. D 82, 094027 (2010). [arXiv:1009.2149].

[64] A. Alexandru and U. Wenger, Phys. Rev. D 83, 034502 (2011). [arXiv:1009.2197].

[65] Y. Iwasaki, UTHEP-118 , (1983), preprint

[66] B. Sheikholeslami, R. Wohlert, Nucl. Phys. B259 (1985) 572.

[67] A. Nakamura, S. Oka, and Y. Taniguchi, JHEP 02 (2016) 054

[68] WHOT-QCD Collaboration, S. Ejiri, Y. Maezawa, N. Ukita, S. Aoki, T. Hatsuda, N. Ishii, K. Kanaya and T. Umeda, Phys. Rev. D 82, 014508 (2010).

[69] A. Li, A. Alexandru and K. F. Liu, Phys. Rev. D **84**, 071503 (2011) [arXiv:1103.3045 [hep-ph]].

[70] A. Alexandru, M. Faber, I. Horvath and K. F. Liu, Phys. Rev. D **72**, 114513 (2005) [hep-lat/0507020].

[71] A. Li, A. Alexandru, K. F. Liu and X. Meng, Phys. Rev. D **82**, 054502 (2010) [arXiv:1005.4158 [hep-lat]].

[72] A. Alexandru, C. Gattringer, H. -P. Schadler, K. Splittorff, J. J. M. Verbaarschot, Phys. Rev. D **91**, 074501 (2015) [arXiv:1411.4143 [hep-lat]].

[73] C. Gattringer, H. -P. Schadler, Phys. Rev. D **91**, 074511 (2015) [arXiv:1411.5133 [hep-lat]].